Seismic structure of the Central Tyrrhenian basin: Geophysical constraints on the nature of the main crustal domains

M. Prada,[1] V. Sallares,[1] C. R. Ranero,[2] M. G. Vendrell,[1] I. Grevemeyer,[3] N. Zitellini,[4] and R. de Franco[5]

[1]   In this work we investigate the crustal and tectonic structures of the Central Tyrrhenian back-arc basin combining refraction and wide-angle reflection seismic (WAS), gravity, and multichannel seismic (MCS) reflection data, acquired during the MEDOC (MEDiterráneo OCcidental)-2010 survey along a transect crossing the entire basin from Sardinia to Campania at 40°N. The results presented include a ~450 km long 2-D P wave velocity model, obtained by the traveltime inversion of the WAS data, a coincident density model, and a MCS poststack time-migrated profile. We interpret three basement domains with different petrological affinity along the transect based on the comparison of velocity and velocity-derived density models with existing compilations for continental crust, oceanic crust, and exhumed mantle. The first domain includes the continental crust of Sardinia and the conjugate Campania margin. In the Sardinia margin, extension has thinned the crust from ~20 km under the coastline to ~13 km ~60 km seaward. Similarly, the Campania margin is also affected by strong extensional deformation. The second domain, under the Cornaglia Terrace and its conjugate Campania Terrace, appears to be oceanic in nature. However, it shows differences with respect to the reference Atlantic oceanic crust and agrees with that generated in back-arc oceanic settings. The velocities-depth relationships and lack of Moho reflections in seismic records of the third domain (i.e., the Magnaghi and Vavilov basins) support a basement fundamentally made of mantle rocks. The large seamounts of the third domain (e.g., Vavilov) are underlain by 10–20 km wide, relatively low-velocity anomalies interpreted as magmatic bodies locally intruding the mantle.

1. Introduction

[2] The Western Mediterranean region is characterized by the formation of back-arc basins associated to rollback of oceanic slabs and the retreat of subduction fronts [*Dewey et al.*, 1989; *Schettino and Turco*, 2011] since Oligocene times. When the rate of slab rollback makes trench retreat to exceed plate convergence rate, extension in the overriding region occurs (e.g., Tyrrhenian basin) [*Nur et al.*, 1993; *Royden*, 1993]. Widespread upper plate extension in the Mediterranean

region has led to lithospheric stretching forming rifted basins like the Valencia through [*Pascal et al.*, 1992; *Gallart et al.*, 1995] that has proceeded locally to full continental breakup and seafloor spreading as in the South Balearic-Algerian basin [*Booth-Rea et al.*, 2007] and the Liguro-Provençal basin [*Rollet et al.*, 2002; *Gailler et al.*, 2009]. Previous WAS work has characterized the continental rift structure of the Northern Tyrrhenian basin [*Contrucci et al.*, 2001; *Contrucci et al.*, 2005; *Moeller et al.*, 2013], and numerous publications have proposed the presence of oceanic crust in the Central Tyrrhenian [e.g., *Faccena et al.*, 2001; *Sartori*, 2003, *Sartori et al.*, 2004; *Cella et al.*, 2008; *Vignaroli et al.*, 2009], but modern geophysical data characterizing the structure and nature of the basement in the central region are lacking to date.

[3] Our study area is the Central Tyrrhenian Sea, which has been previously studied with geophysical and geological studies that reported a complex crustal structure. A stretched continental crust in the Sardinia and Italian margins has been interpreted from MCS images and sampling of basement highs (Figure 1b) [*Colantoni et al.*, 1981; *Kastens and Mascle*, 1990; *Finetti et al.*, 2001; *Sartori et al.*, 2001, 2004]. Several low-resolution seismic refraction experiments carried out between the 1960s and the 1980s (Figure 1a)

[1]Barcelona Center for Subsurface Imaging, ICM, CSIC, Barcelona, Spain.
[2]Barcelona Center for Subsurface Imaging, ICM, ICREA at CSIC, Barcelona, Spain.
[3]GEOMAR Helmholtz Centre for Ocean Research Kiel, Kiel, Germany.
[4]Istituto Scienze Marine, CNR, Bologna, Italy.
[5]Istituto per la Dinamica dei Processi Ambientali, CNR, Milano, Italy.

Corresponding author: M. Prada, Barcelona Center for Subsurface Imaging, ICM, CSIC, Passeig Marítim de la Barceloneta, 37–49, Barcelona ES-08003, Spain. (mprada@icm.csic.es)
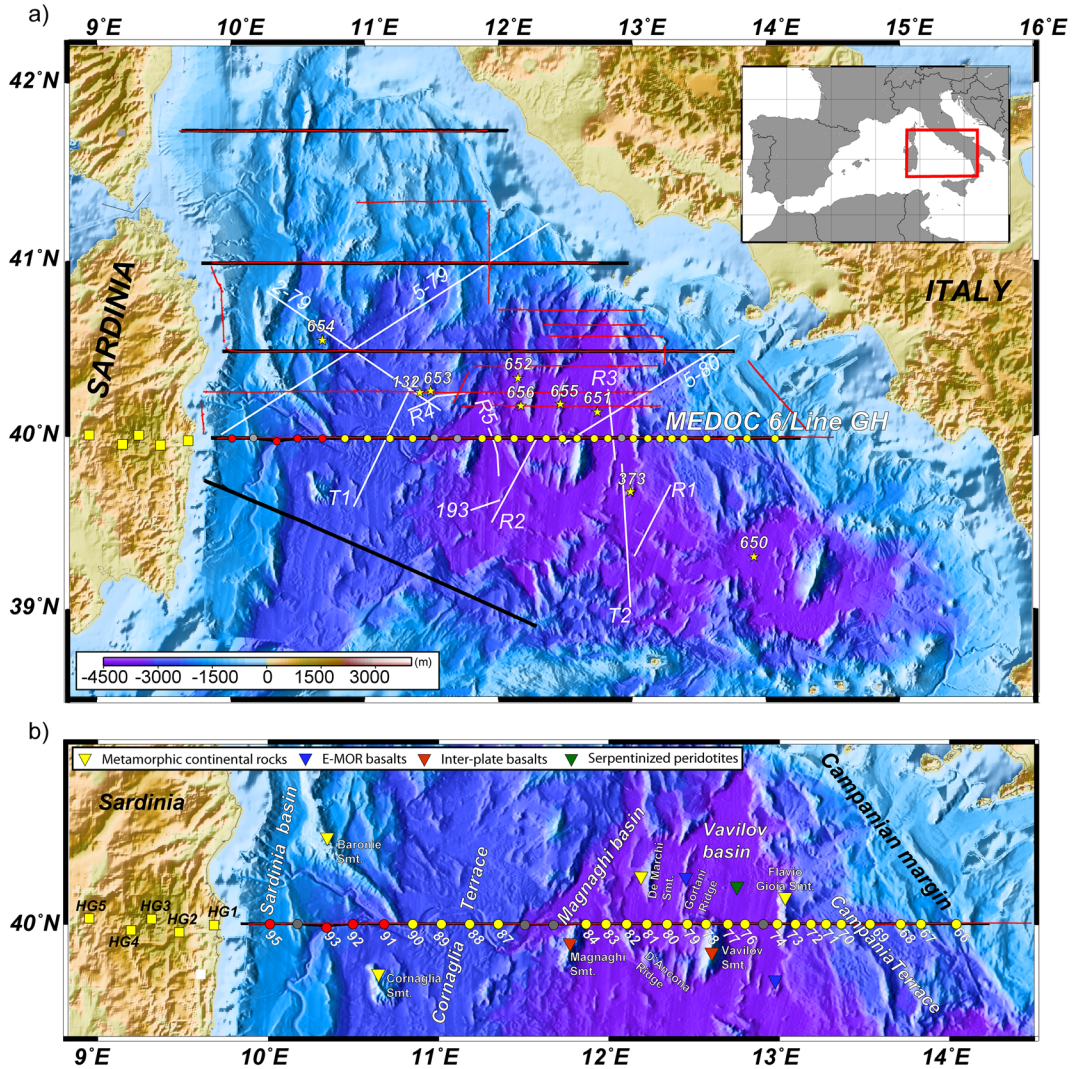
Figure 1. (a) Bathymetric and topographic map of the Tyrrhenian Sea region, located in the Central Mediterranean (see inset). The black and red lines correspond to the WAS and MCS profiles acquired during the MEDOC (MEDiterráneo OCcidental) survey, respectively. The Land-stations (yellow squares), OBSs (red circles) and OBHs (yellow circles) used to obtain the tomographic model of Line GH (Figure 3a) are also shown in the image. Grey circles correspond to both OBSs and OBHs that came out without valid data. White lines correspond to the old seismic refraction experiments carried out between the 60's and 80's, and mentioned in the text [*Fahlquist and Hersey*, 1969; *Nicolich*, 1981; *Recq et al.*, 1984; *Duschenes et al.*, 1986]. Yellow stars correspond to the location of the ODP and DSDP sites [*Dietrich et al.*, 1977; *Kastens and Mascle*, 1990]. (b) Close-up of the study area with the location of the main morphological features. Colored triangles represent the petrological nature of the basement at those points of interest for this work [*Dietrich et al.*, 1977; *Colantoni et al.*, 1981; *Kastens and Mascle*, 1990; *Sartori et al.*, 2004].

provide 1-D velocity models that were interpreted as showing stretched continental crust under the Cornaglia Terrace (Figure 1b) and oceanic crust under the Magnaghi and Vavilov basins (Figure 1b) [*Fahlquist and Hersey*, 1969; *Nicolich*, 1981; *Recq et al.*, 1984; *Duschenes et al.*, 1986; *Sartori et al.*, 2004]. Ground truthing of the nature of the basement was achieved by Deep Sea Drilling Project (DSDP) Leg 42A and Ocean Drilling Program (ODP) Leg 107 (Figure 1b). Drilling found enriched mid-ocean ridge (E-MOR) basalts at the top of the Gortani Ridge (ODP site 655 in Figure 1b) and in the Vavilov basin (ODP site 651 and DSDP site 373 in Figure 1b) [*Barberi et al.*, 1978;

Dietrich et al., 1977; *Beccaluva et al.*, 1990; *Bertrand et al.*, 1990]. Drilling of the top of the basement under about 1 km of sediment of the Vavilov basin found few tens of meters of basalt, but deeper drilling found serpentinized peridotites (ODP site 651 in Figure 1b) [*Bonatti et al.*, 1990; *Kastens and Mascle*, 1990]. Regional compilations of Moho depth also show a heterogeneous crustal structure [*Steinmetz et al.*, 1983; *Gvirtzman and Nur*, 2001; *Di Stefano et al.*, 2011] but lack the appropriate resolution to understand basin structure, so that the spatial distribution and the nature of the main geological domains remain unconstrained.

[4] The main goal of this work is to fulfill this lack of knowledge and define the petrological affinity of the different basement domains across the basin. For this we use WAS and gravity models combined with MCS data, all acquired during the MEDOC-2010 experiment. Specifically, we present results from a ~450 km long WAS and gravity profile and a coincident MCS line acquired across the Central Tyrrhenian basin, at ~40°N (Figure 1). We show the 2-D velocity model of the WAS Line GH, the corresponding velocity-derived density model that matches the measured gravity anomalies, and the coincident MCS profile MEDOC-6 (Figure 1), which in this work is essentially used as a complement to help defining the crustal structure and boundaries between the petrological domains. A joint refraction and reflection traveltime inversion model of the WAS data together with the MCS image have allowed to determine the velocity structure, the main tectonic features, and the geometry of the crust-mantle boundary across the entire basin. The comparison of the velocity model with existing velocity compilations of different crustal types, together with results from gravity modeling, provides novel information that addresses the petrological nature of the geological domains, and the transition between them in the Central Tyrrhenian basin in an unprecedented detail. These results provide new insights that will surely help to further understand fundamental questions on the mechanisms of continental extension and rifting in back-arc oceanic settings.

2. Geodynamic and Tectonic Setting

[5] The Tyrrhenian Sea is a Neogene back-arc basin surrounded to the east and south by an arcuate orogenic system formed by the Apennines in the Italian Peninsula, the Calabrian Arc in Southern Italy, and the Maghrebides in Sicily and northeastern Africa, and to the west by the Sardinia-Corsica block.

[6] The evolution of the Tyrrhenian basin together with the orogenic system and the Liguro-Provençal basin is linked to the east-southeastward migration of the Apennines-Calabrian subduction system [*Malinverno and Ryan*, 1986]. Trench retreat and formation of back-arc basins in the Mediterranean region started during the Oligocene at ~33 Ma [*Schettino and Turco*, 2011]. The Liguro-Provençal basin formed ~30–23 Ma leading to oceanic spreading in the central parts in response to the 25°–30° counterclockwise rotation of the Corsica–Sardinia block that occurred ~20–15 Ma [*Gattacceca et al.*, 2007]. Extension stopped in the Liguro-Provençal basin and shifted to the Tyrrhenian region during intra-Tortonian time affecting a region occupied by the Alpine and the Apenninic orogenic belts [*Trincardi and Zitellini*, 1987; *Mascle and Rehault*, 1990; *Sartori*, 1990, 2001]. From Tortonian to late Messinian eastward migration of the subduction front caused E-W contemporaneous back-arc extension in the Tyrrhenian region [*Faccena et al.*, 2001]. Between ~6 and 5 Ma the style of subduction rollback experienced major changes. In the Northern Tyrrhenian, it is suggested that the underthrusting of positively buoyant continental crust into the subduction system caused a progressive slow down of rollback [*Faccena et al.*, 2001]. In contrast, the Central and Southern Tyrrhenian basin underwent larger amount of extension due to the migration of the subduction front southeastward under the Calabrian arc [*Faccena et al.*, 2001].

[7] From a morphotectonic point of view, the Tyrrhenian Sea can be subdivided in three different domains (Figure 1); the Northern (north of ~40° 45′N), which displays shallower seafloor and rough morphology; the Central (from ~40° 45′N to ~39°N) with deeper seafloor and extended abyssal plains spotted with prominent volcanic and nonvolcanic seamounts, and the Southern Tyrrhenian with the volcanic arc along the Sicilian-Calabrian margin. The Northern Tyrrhenian basin system of normal faults trends roughly N-S to turn NW-SE to the east [*Mauffret and Contruccci*, 1999; *Moeller et al.*, 2013]. This basin is spotted by small-scale magmatic intrusions [*Moeller et al.*, 2013] that decrease in age eastward [*Bartole*, 1995]. The Corsica basin in the westernmost Northern Tyrrhenian, initiated during the counterclockwise rotation of Corsica and Sardinia at least 20 Ma [*Zitellini et al.*, 1986; *Mauffret and Contruccci*, 1999]. However, most normal faulting in the northernmost sector of the Northern Tyrrhenian was produced from Tortonian to mid-Pliocene time [*Mauffret and Contruccci*, 1999] during the opening of the Tyrrhenian.

[8] Previous works interpreted that in the Central Tyrrhenian apparently higher extension factors caused the formation of oceanic crust in the Magnaghi, Vavilov, and Marsili basins (Figure 1b) [*Duschenes et al.*, 1986; *Kastens and Mascle*, 1990; *Sartori*, 1990, 2003; *Faccena et al.*, 2001; *Sartori et al.*, 2004]. The Central Tyrrhenian is also the locus of the several kilometers tall volcanic edifices of Magnaghi, Vavilov, and Marsili seamounts (Figure 1b), attributed to an upper Pliocene to present-day volcanism [*Savelli*, 1988, 2002; *Lustrino et al.*, 2011].

3. Geophysical Data Sets and Methodology

[9] During the MEDOC-2010 survey a total of 17 MCS (2800 km) and 5 WAS profiles were acquired with the Spanish R/V *Sarmiento de Gamboa* and the Italian R/V *Urania* and were also recorded by several land stations installed in Corsica and Sardinia (Figure 1).

3.1. Wide-Angle Seismic Data

[10] The GH WAS line extends from Sardinia to the Campania margin across the deepest parts of the Tyrrhenian basin (Magnaghi and Vavilov basins) (Figure 1b). These data were recorded by 4 Spanish *LC2000 4×4* ocean bottom seismometers (OBS) deployed by the R/V *Sarmiento de Gamboa*, 22 German *E-2PD* and *HTI-01-PCA* ocean bottom hydrophones (OBH) deployed by the R/V *Urania*, and 5 Italian onshore *Lennartz M24-LP-24 bit* seismometers installed in Sardinia. Average receiver spacing along the line was ~10 km. The R/V *Sarmiento de Gamboa* seismic source consisted of two arrays of six G-II air guns each, with a total capacity of 4600 in^3, fired at constant interval of 90 s (~220 m). The signal-to-noise ratio for the OBS data was high, and therefore, a Butterworth band-pass filter (5–15Hz) and an automatic gain control (AGC) were applied. OBH data processing included a predictive deconvolution, a Butterworth band-pass filtering (2–11Hz), and an AGC. For the high-quality land receivers a Butterworth band-pass filtering (3–13Hz) was only applied.

[11] Four types of seismic phases have been interpreted in the record sections (Figure 2), three refraction phases within the crust (Pg), the basement (Pb), and uppermost mantle (Pn), and a crust-mantle boundary reflection (PmP). In average,
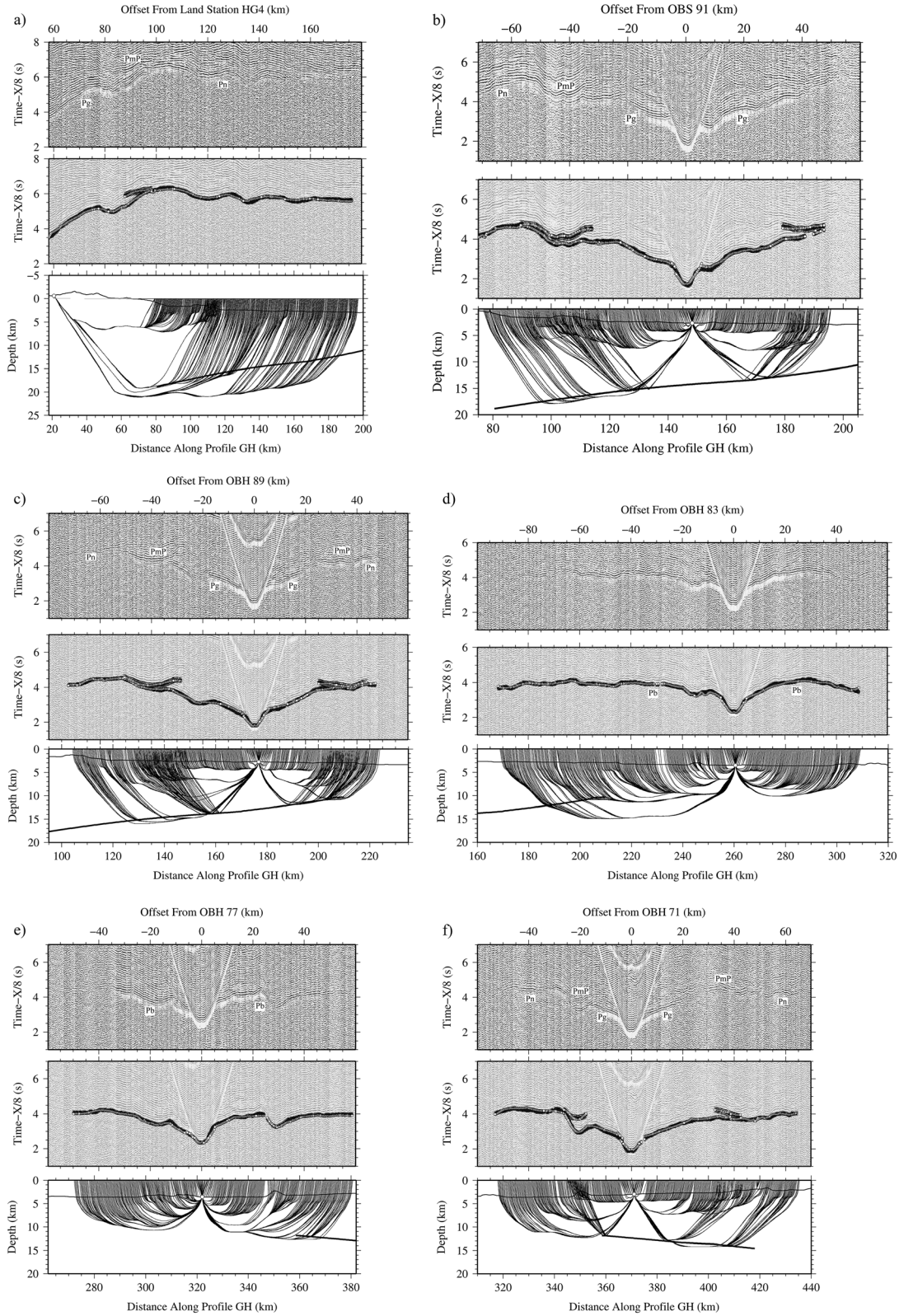
Figure 2. From top to bottom, record section, data fit, and ray-tracing of (a) land station HG4, (b) OBS 91, (c) OBH 89, (d) OBH 83, (e) OBH 77, and (f) OBH 71. The main seismic phases recognized in land station HG4, OBS 91, and OBHs 89 and 71 are the refracted phases through the crust (Pg) an uppermost mantle (Pn), and the reflections at the crust-mantle boundary (PmP). While in OBHs 83 and 77, no PmP phases are recognized, and only a refracted phase through the basement (Pb) with an apparent velocity of ~8 km/s is discerned. In the data fit panels, the black and white circles correspond to the picked and calculated data, respectively. While the thick black line in the ray-tracing panels represents the inverted Moho geometry, and the white circle the receiver location.
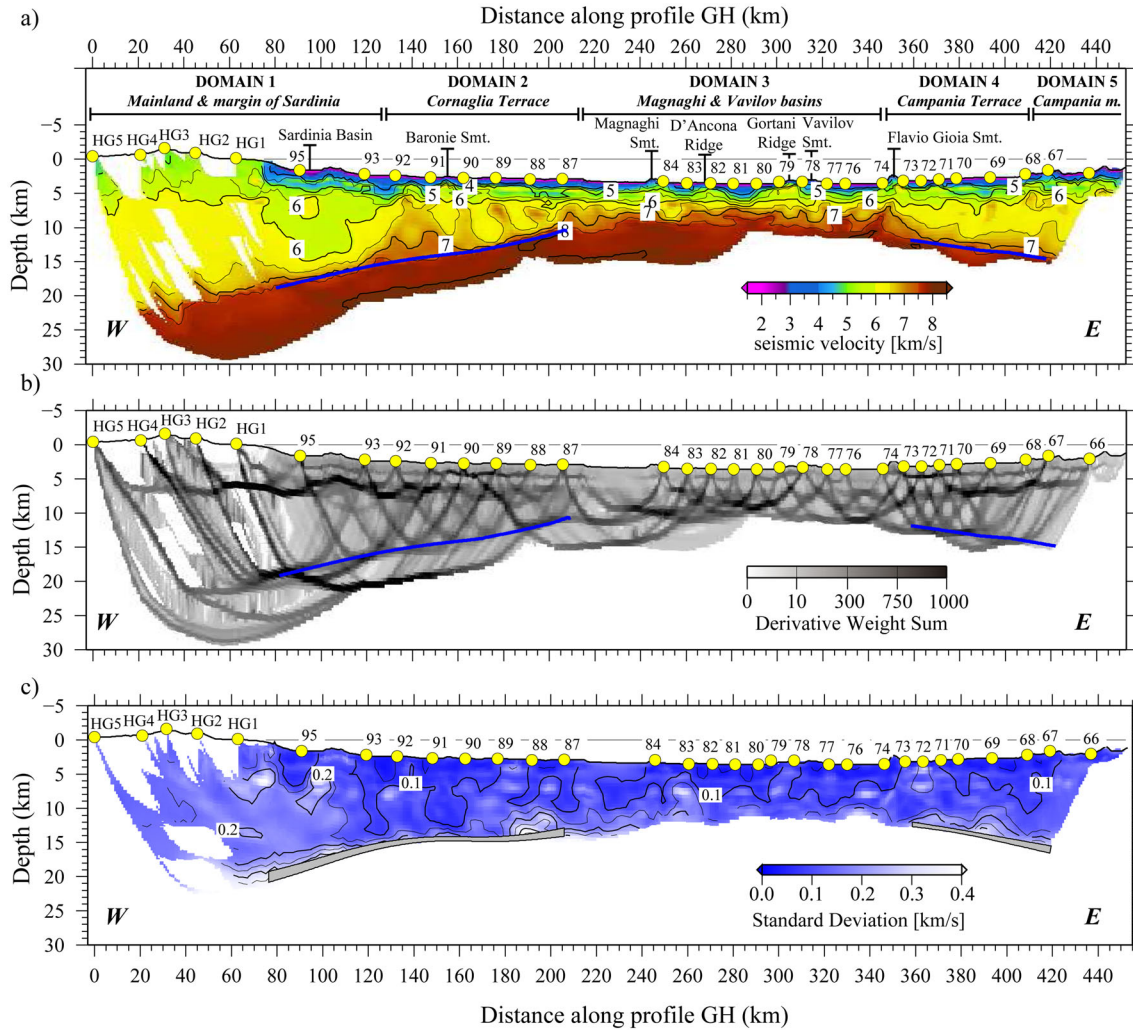
Figure 3. (a) Final *P* wave velocity model of the crust, uppermost mantle and Moho geometry along the WAS line GH. The model was obtained by inverting the Pg, Pn, Pb, and PmP phases with the joint reflection and refraction traveltime tomography *tomo2d* code [*Korenaga et al*., 2000]. Campania m.: Campania margin. (b) Derivative weight sum (DWS) values of the above tomographic model in Figure 3a. Blue line in both Figures 3a and 3b represents the inverted Moho geometry. (c) Final standard deviation values for the *P* wave velocity values and the Moho geometry (grey band), as a result of the statistical uncertainty analysis. Note that in this analysis the mantle is not included. Details of the calculation are given in the text. Yellow circles display the location of the land stations, OBHs, and OBSs used in this work.

land stations display a ~40 km long Pg phase with apparent velocities ranging from 6.0 to 6.5 km/s (Figure 2a), a Pn phase from km ~40 to ~110 with a mantle-like apparent velocity of >7 km/s, and energetic PmP reflections (Figure 2a). The same phases are observed in OBS 95 to OBH 87 located in the Sardinia margin and the Cornaglia Terrace (Figures 2b and 2c). These OBS-OBH stations show Pg arrivals in 40–50 km offset range with 6.0–6.5 km/s apparent velocities and faster Pn phases with >7 km/s apparent velocity. Most of these record sections display a secondary arrival corresponding to PmP reflections, indicating an abrupt crust-mantle velocity boundary. Conversely, OBHs 84 to 74 located in the central part of the basin under the Magnaghi and Vavilov basins display no PmP phase (Figures 1b, 2d, and 2e). Here we interpret a single refracted phase (Pb) through the basement, because it is not evident

how to distinguish between crustal and upper mantle refractions. This Pb phase is observed up to 90 km offset with unusually high apparent velocity of > 7 km/s at short offsets in most OBH records. In this region, only OBH 77 (Figure 2e), 78, and 79 show Pb phases with slower 5–6 km/s apparent velocities along their ~30 near-offset kilometer, located across the Gortani Ridge and Vavilov seamount. From OBH 73 to 66 across the terrace and margin of Campania (Figure 1b), seismic phases changes displaying a configuration that resembles to that of the conjugate Sardinia margin, with moderate-velocity Pg phases in the ~40 km offset range, mantle-like velocity Pn phases, and clear, high-amplitude PmP phases (Figure 2f).

[12] A total of 14,403 first arrivals (Pg, Pb, and Pn) and 1877 PmP reflections were manually picked. A picking error of one half of the dominant period was assumed accounting
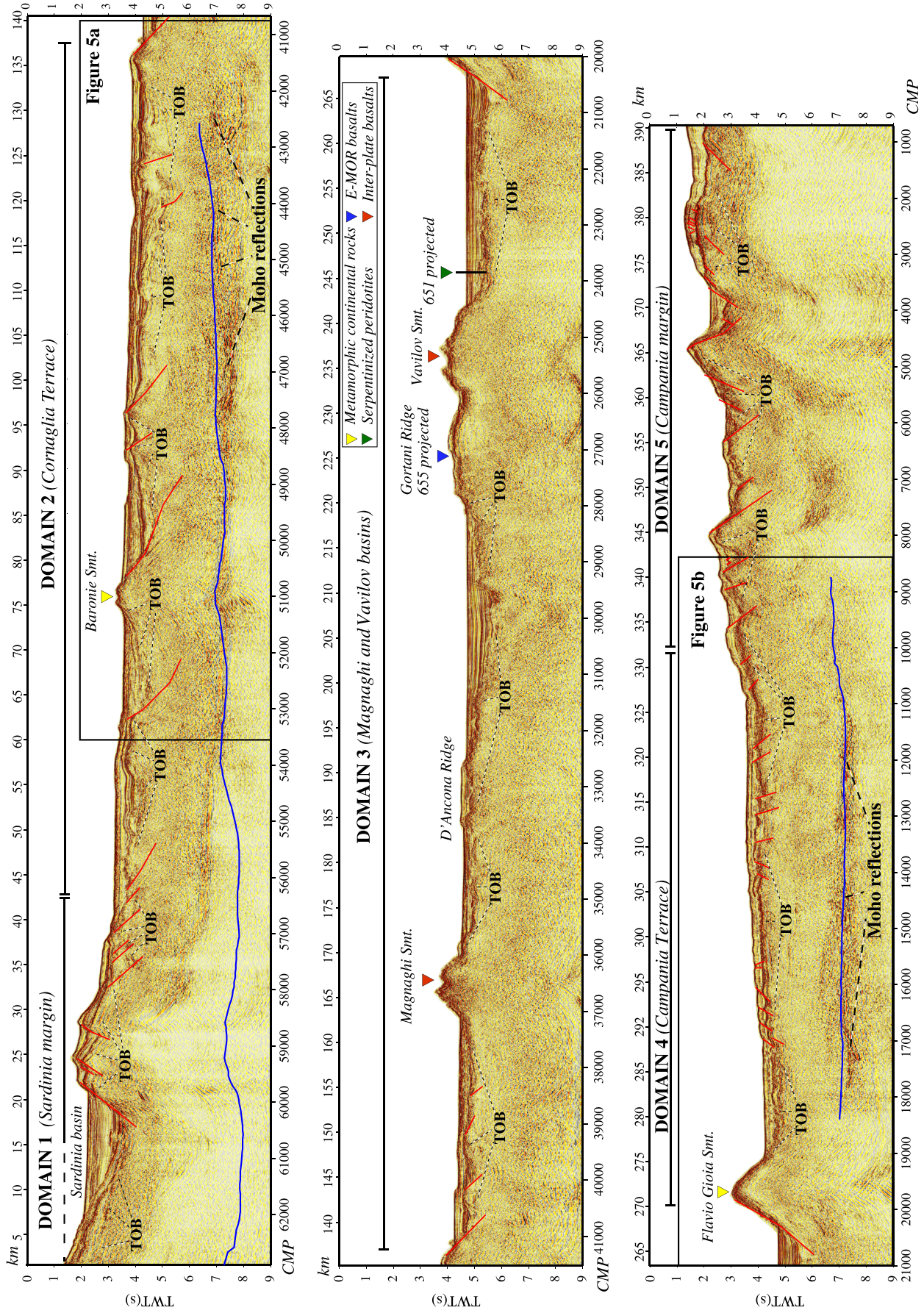
for a possible systematic shift in arrival identification. We assume that picking uncertainty ranges between 40 and 50 ms for Pg, Pb, and Pn and 60 ms for PmP.

3.1.1. Seismic Tomography and Uncertainty Analysis

[13] To model the WAS data we used the joint refraction and reflection traveltime inversion code *tomo2d* [*Korenaga et al.*, 2000], which allows obtaining a 2-D velocity grid and the geometry of a floating reflector. The grid consists of a field of nodes hanging from the seafloor with variable spacing in the vertical and horizontal directions. The floating reflector is represented by one array of (x, z) coordinates that is independent from the velocity grid. The synthetic traveltimes of the inverted phases are calculated by integration along the calculated raypaths. Ray tracing is done with the graph method [*Moser*, 1991] in a first stage with a subsequent ray-bending refinement [*Moser et al.*, 1992]. Smoothing constraints are applied for both velocity and reflector geometry parameters, by means of laterally and vertically variable correlation lengths. Additionally, damping constraints are used to regularize the linear system and stabilize the inversion. Our model domain is 450 km wide and 35 km deep, with node spacing varying in the vertical component from 0.125 km at the seafloor to 1.5 km at the bottom, and a constant spacing of 0.5 km in the horizontal. Node spacing for the floating reflector is also 0.5 km and constant. In order to select the most appropriate set of regularization constraints, several combinations of correlation lengths, damping and smoothing parameters were tested. According to test results we choose a horizontal correlation length of 2 km at the top and 8 km at the bottom, and a vertical correlation length of 0.2 km at the top and 1.5 km at the bottom.

[14] To obtain the 2-D velocity model we performed a top-to-bottom layer stripping strategy as indicated in *Sallarès et al.* [2011, 2013a]. The sedimentary layers in this region are too thin to be identified and inverted using the WAS data; thus, we started inverting sediments and crust at once using Pg/Pb and PmP phases to account for the crustal velocity field and the location and geometry of the crust-mantle boundary reflector. In a second stage we used the crustal velocity model as initial model and incorporated Pn phases in the inversion to define the uppermost mantle velocity field. The starting depth for the crust-mantle boundary was set at 15 km depth below the Sardinia and the Campania margins and at 25 km below the Sardinia Island [*Moeller et al.*, 2013].

[15] The velocity nodes above the Moho reflector were overdamped in order to boost the changes below the crust-mantle boundary. The final 2-D velocity model was obtained after 10 iterations with a root-mean-square (RMS) of 68 ms and a chi-square value (χ^2) of 1.2. The RMS is 69 ms for the Pg, Pb, and Pn phases and 59 ms for the PmP. The ray coverage in the model is represented by the derivative weight sum (DWS) [*Toomey and Foulger*, 1989], which is a measure of the linear sensitivity of the inversion (Figure 3b).

[16] To estimate model parameters uncertainty due to combinations of picking errors and starting velocity model we performed a nonlinear Monte Carlo-type error analysis.

This method is similar to that used in *Sallarès and Ranero* [2005], which is in turn a modified version of that used in *Korenaga et al.* [2000]. The approach consists of randomly perturbing the velocity values of the initial model and the depth of the Moho reflector within a priori reasonable bounds (σ_v = 0.75 km/s and σ_z = 2 km), to create a set of 250 2-D reference models and their modified reference Moho reflectors. In addition, 250 noisy traveltime data sets were constructed by adding a random timing error of ± 65 ms, which includes the potential influence of common phase errors (±25 ms), common receiver errors (±25 ms), and individual picking errors (±15 ms). We inverted randomly selected pairs of perturbed reference models and reflector, and noisy data sets. The mean deviation of all the solutions (Figure 3c) is then taken as a measure of the model parameters (velocity and reflector's geometry) uncertainty [*Tarantola*, 1987].

3.2. Gravity Modeling

[17] We have compared several density models calculated from inverted velocities using different empirical velocity-density (Vp-ρ) relationships to see which of them explain better the measured gravity data (i.e., recorded during the MEDOC survey). This approach helps discerning between interpretations of the nature of rocks based on seismic velocity only [*Korenaga et al.*, 2001; *Sallarès et al.*, 2000; *Sallarès and Ranero*, 2005].

[18] The Vp-ρ relation used to convert velocities (Figure 3a) into densities for sediment is *Hamilton*'s [1978] law for shale. For the basement, we tested three different relationships corresponding to continental crust, oceanic crust, and exhumed mantle. For continental crust we used *Christensen and Mooney*'s [1995] relationship, for oceanic crust layers 2 and 3 basalts and gabbros we employed *Carlson and Herrick*'s [1990], and for mantle rocks we used *Carlson and Miller*'s [2003] relation for low-T serpentinized peridotite. To correct from laboratory to in situ conditions, and vice versa, temperature and pressure derivatives of the P wave velocity were applied for oceanic crust [*Korenaga et al.*, 2001] and for serpentinized peridotites (sample T-580 in *Kern and Tubia* [1993]). For the 2-D gravity modeling we used a code based on *Parker* [1972] spectral method implemented by *Korenaga et al.* [2001]. This method allows calculating the gravity anomaly produced by a vertically laterally heterogeneous density model.

3.3. Multichannel Seismic Profile

[19] The ~400 km long MCS MEDOC-6 line was acquired with a 276 channel, 3450 m long streamer, on board the Spanish R/V *Sarmiento de Gamboa*. The seismic source consisted of nine G-II air guns with a total capacity of 3040 in.[3] fired every 50 m, yielding a common midpoint (CMP) fold of 35.

[20] Data were processed using Globe Claritas software to obtain the section in Figures 4–6. The main steps during processing included spherical divergence correction, two-

---

Figure 4. Poststack time migration of profile MEDOC 6. The tectonic structure of the curst along this section is mainly represented by landward and seaward normal faults (red lines). Worth to be noted is the excellent correlation between the interpreted Moho along the MCS profile and that obtained by the inversion of PmP phases (blue line). The colored triangles are the same used in Figure 1b to indicate the nature of the basement inferred from rock sampling [*Dietrich et al.*, 1977; *Colantoni et al.*, 1981; *Kastens and Mascle*, 1990; *Sartori et al.*, 2004]. TOB: top of basement.
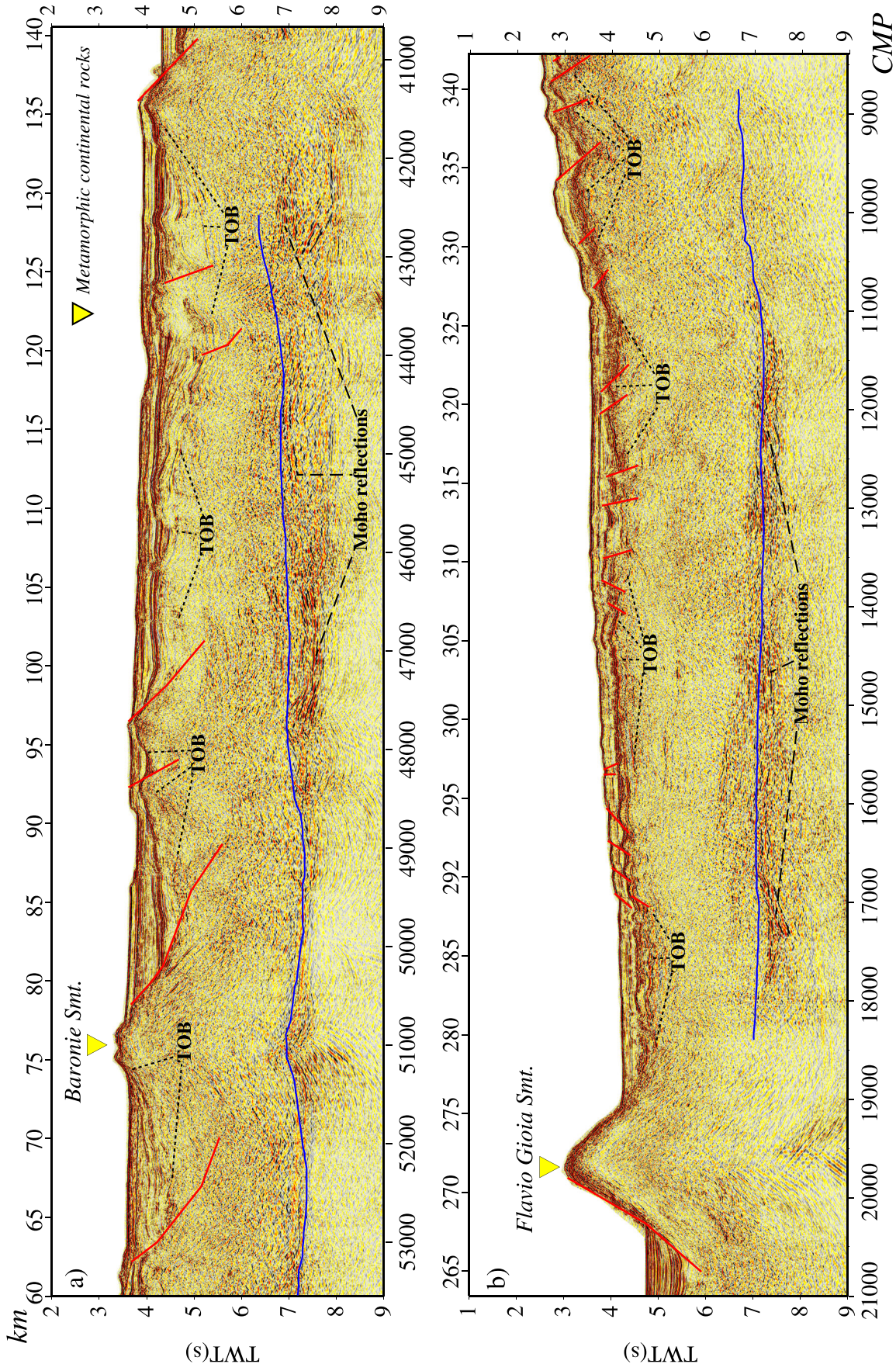
window statistical deconvolution, prestack multiple removal with parabolic radon filtering, normal move out, near and far offset mute, stack, poststack frequency-wavenumber noise attenuation, poststack finite difference time migration, time- and space-variant band-pass frequency filtering following the geological structure, followed by two-window time-variant automatic gain control for amplitude balancing.

4. Results

4.1. Velocity Structure

[21] The main characteristics of the velocity model in Figure 3a are the laterally variable marine sediment layer, the heterogeneous basement velocity structure showing a strong vertical velocity gradient at its upper part, and the progressive crustal thinning toward the center of the basin. Based on the velocity structure we propose the presence of five different domains.

[22] Domain 1 extends from 0 to ~125 km (Figure 3a) and includes mainland Sardinia (0–80 km) and the Sardinia margin (80–125 km). Here the model displays the 2.0–2.5 km deep Sardinia basin (Figures 3a and 6), with Vp of ~1.8 km/s at the top to 3.5–4.0 km/s at the base (Figure 6). Under the sedimentary basin, the upper 2–3 km of the basement are characterized by a strong velocity gradient of ~0.5 s^{-1}, underlain by a lower velocity gradient with velocity at middle- and lower crustal levels of 5.5–6.5 km/s. The Moho of domain 1 is well constrained by PmP reflections between ~80 to ~125 km along the profile in Figure 3a, showing a significant shoaling from 20–21 km depth at ~80 km to ~15 km depth at ~125 km along profile, defining a significant crustal thinning (Figure 3a).

[23] Domain 2 extends from ~125 to ~210 km (Figure 3a) and corresponds to the Cornaglia Terrace (Figure 1b). Similar to domain 1, the underlying uppermost 2–3 km of basement have a vertical velocity gradient of ~0.5 s^{-1}, whereas middle- and lower crustal velocities are higher than in domain 1, ranging between 6.5 km/s at the top and 7.1–7.2 km/s at the bottom (Figure 3a). The Moho is well constrained by clear PmP phases in WAS data, and it is also visible in the MCS line (Figures 4 and 5). It shoals from ~15 km to 10 km depth between ~125 and ~210 km along profile (Figure 3a). The basement velocity structure also displays abrupt lateral contrasts of about 0.5 km/s that delineate four 10–15 km wide, subvertical structures with velocity ranging between 6.0 km/s and 6.5 km/s (between OBH 91 and 87 in Figure 3a).

[24] Domain 3 extends from ~210 to ~345 km along profile (Figure 3a). This region is characterized by the absence of wide-angle Moho reflections (no PmP between OBH 84 and OBH74). Similarly, the MCS images that show Moho reflections in other domains do not display clear reflections at the expected Moho TWT in domain 3 (Figures 4 and 6).

The Vp model displays here the strongest vertical velocity gradient (≥1 s^{-1}), twice as strong as in any other domain. The base of the 1–2 km thick sediment cover of Magnaghi and Vavilov basins, well imaged on MCS data (Figure 4), corresponds to the 3.5–4.0 km/s contours (Figure 6). The basement is not bounded at its base by PmP reflections, and it is well resolved by the dense coverage of Pb phases in Figure 3b. The velocity structure shows a gradual increase from ~4.0 to 4.5 km/s near the top of basement to 8 km/s at the deepest well-resolved part of the model at ~7–10 km depth, i.e., 4–5 km below the top of the basement. In average, the vertical velocity gradient in these uppermost ~5 km of the basement is twice stronger than in domain 2 and even more compared with that of domain 1. Coinciding with the bathymetric highs of Magnaghi seamount, and the profile intersections with the D'Ancona and Gortani Ridges and the Vavilov seamount (Figures 1b and 3a), the model shows four velocity anomalies extending from the top of the basement to about 10 km depth (r1-r4 in Figure 10). Compared to the rest of domain 3, these anomalies have gentler vertical velocity gradient, faster velocity at shallow levels, and slower velocity at deep levels. These local anomalies are better displayed by comparing vertical velocity gradients rather than absolute velocities (Figure 10b) (see section 5.4 for details).

[25] Domain 4 encompasses the Campania Terrace, from ~350 to 410 km (Figures 1b and 3a). Here PmP reflections are clear in the record sections (Figure 2f), constraining well the Moho geometry. Crustal thickness increases from ~7 to ~10 km from 355 to ~410 km along profile (Figure 3a). The basement velocity structure is similar to domain 2, with Vp increasing from 4.0–4.5 km/s at the top to 7.1–7.2 km/s at the base of the crust. However, the velocity distribution of domain 4 is more homogeneous laterally, without the subvertical velocity structures observed in domain 2 (Figure 3a).

[26] Domain 5 runs across the Campania margin (i.e., last 30–40 km of profile in Figure 3a). Here the crustal structure is just moderately well resolved because the ray coverage is poorer. However, the reduction in crustal velocities and the increment of crustal thickness complemented with a significant change of the bathymetry relief suggest that it may represent a change in crustal structure; hence, a fifth domain is interpreted.

[27] Mantle velocity structure is well resolved along the entire line. Beneath mainland and Sardinia margin (domain 1) long-offset Pn phases recorded in the land-stations dive 5–10 km into the mantle (Figure 2a). Clear Pn phases on OBH and OBS records along domains 2 and 3 (Figures 2b and 2e) constrain well the mantle velocity, whereas the Campania margin (domain 4) has limited ray coverage so that mantle velocity is less well resolved (Figure 3b). Overall, velocity under the Moho increases with depth from ~7.6 km/s just under the crust-mantle

Figure 5. (a) Close-up of the MCS profile in Figure 4 along the Cornaglia Terrace. The main features of this region include the coincident absence of both, the inverted Moho (blue line) and the interpreted one along the MCS profile at ~135 km of the profile MEDOC 6, and the presence of seaward normal faults (red lines). The yellow triangle represents the petrological nature of the Baronie seamount [*Kastens and Mascle*, 1990; *Sartori et al.*, 2004]. (b) Close-up of Figure 4 along the Terrace and margin of Campania. As in the Cornaglia Terrace in Figure 5a, the location of the Moho interpreted along this region of the MCS profile and that obtained by the inversion (blue line) coincide remarkably well. The yellow triangle indicates the continental nature of the Flavio Gioa seamount [*Colantoni et al.*, 1981; *Kastens and Mascle*, 1990]. TOB: top of basement.
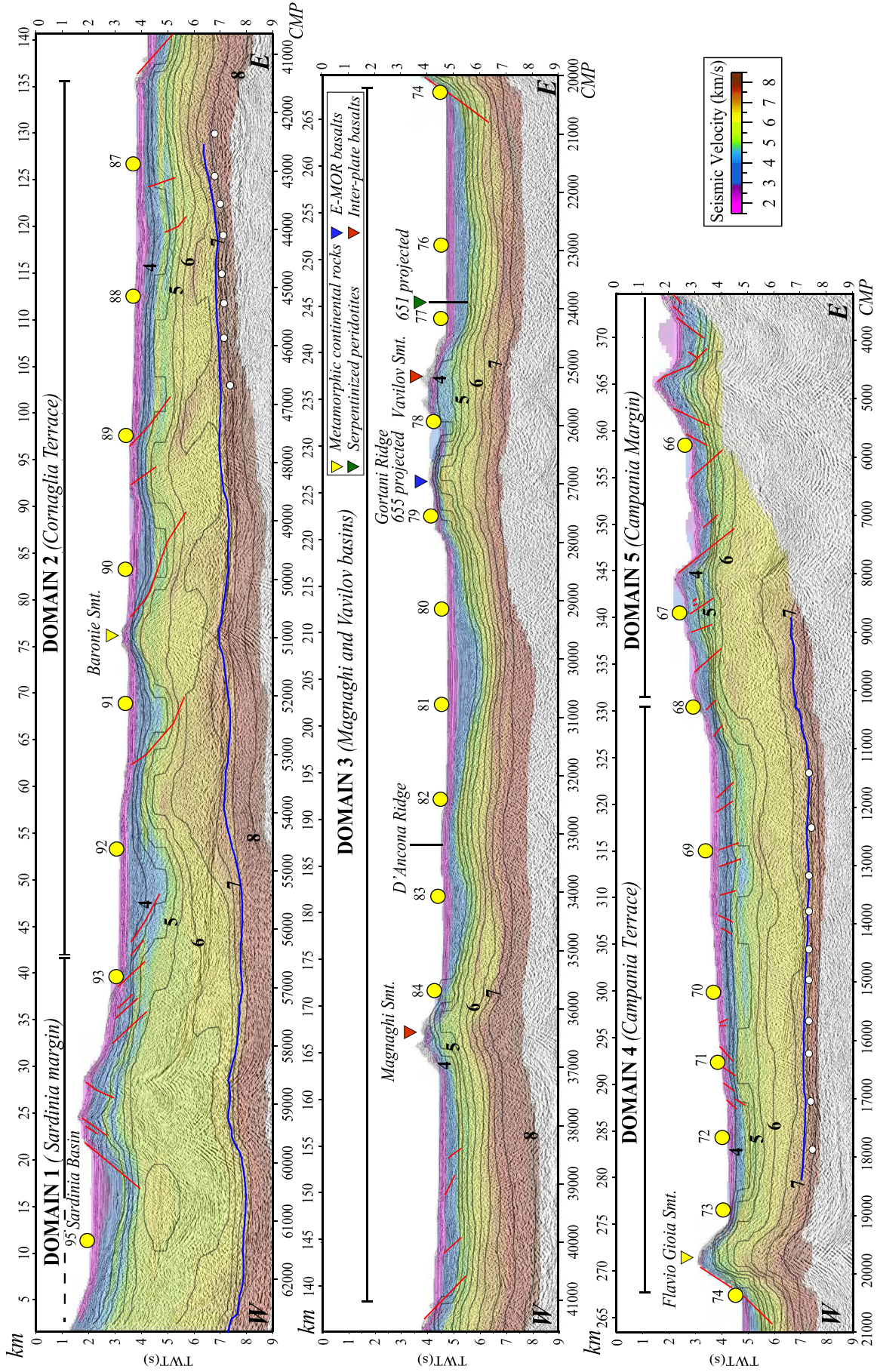
Figure 6. Poststack time migration of profile MEDOC 6 with the same tectonic interpretation as in Figure 4 and overlaid with the two-way time (TWT) converted version of the *P* wave seismic velocity model (Figure 3a). Yellow circles display the location of the OBSs and OBHs along the profile. Colored triangles are the same used in Figure 4 [*Dietrich et al.*, 1977; *Colantoni et al.*, 1981; *Kastens and Mascle*, 1990; *Sartori et al.*, 2004]. White circles display the location of those reflections interpreted as the crust-mantle boundary.
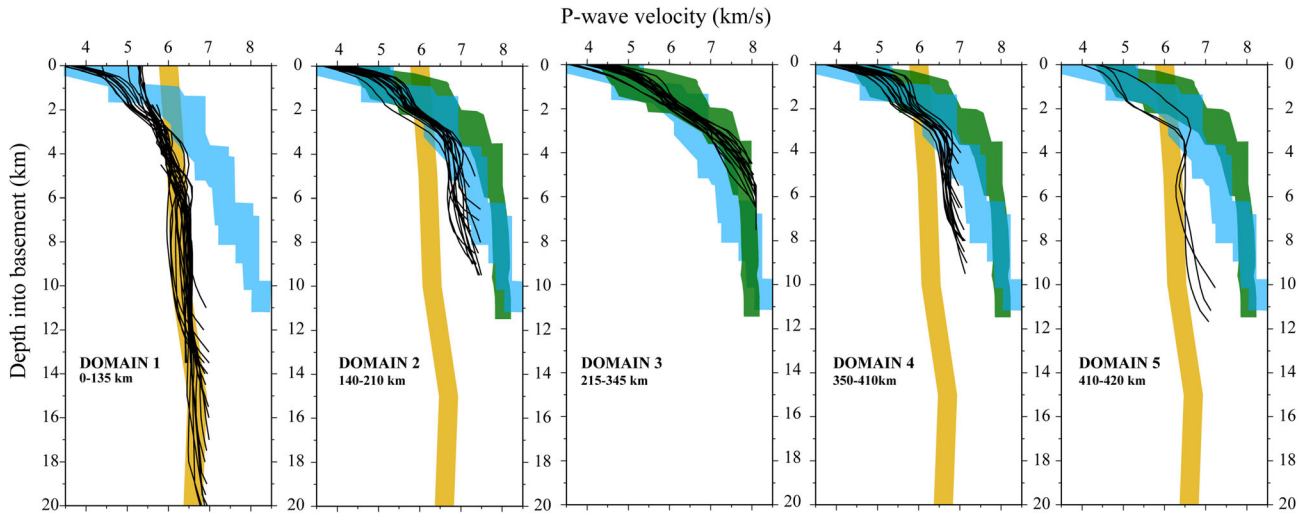
P-wave velocity (km/s)

Figure 7. The 1-D *P* wave velocity-depth profiles of the five differentiated domains along the tomographic model (Figure 3a). Black lines represent the 5 km laterally averaged 1-D velocity-depth profiles extracted from the tomographic model. The 1-D velocity-depth profiles of reference include a 20 km thick continental crust (orange band) [*Christensen and Mooney*, 1995], 0–7 Ma Atlantic oceanic crust (blue band) [*White et al.*, 1992], and a compilation of the exhumed mantle regions found West Iberia (green band) [*Dean et al.*, 2000; *Sallarès et al.*, 2013b].

boundary to ~8.0 km/s ~5 km below, indicating low uppermost mantle velocity in all domains (Figure 3a).

4.1.1. Uncertainty Analysis

[28] Crustal velocity and Moho depth uncertainty of the velocity model in Figure 3a is displayed in Figure 3c. Uncertainty values range between ±0.1 km/s and ±0.2 km/s in most of the model, except under Sardinia, where velocity uncertainty is between ±0.2 km/s and ±0.3 km/s due to low ray coverage (Figure 3b). Velocity uncertainty is also ±0.2 km/s at some locations with strong velocity gradient or contrast, like at ~15 km depth between OBH 87 and 88 and below OBH 69 (Figure 3c). This effect has been observed in other studies [*Sallarès et al.*, 2011, 2013b] around the sediment-basement boundary where there is a sharp velocity contrast. Depth uncertainty for the Moho is small, ranging between ±0.2 km where crustal velocity is constrained by Pg and Pb phases and ±1.3 km where crustal velocity is primarily controlled by PmP phases only, and the depth-velocity trade-off is higher (Figure 3c).

4.2. Tectonic Structure

[29] The MCS seismic image coincident with the WAS profile has been used to define the tectonic structure and to map the presence/absence of Moho in the near-vertical seismic reflection image (Figure 4). The poststack time migration image of MEDOC-6 displays well the sediment cover, the top of basement (TOB), and local groups of reflections from the lower crust that possibly delineate the transition to the Moho at their base (Figure 4). The Vp model has been converted to two-way time (TWT) and overlaid on the seismic image to directly compare the structure obtained by the two methods (Figure 6). Overall, there is a regional good correspondence between structures in both images, but the two methods appear to have mapped some structures in different

ways, which may give information on the nature of rocks forming the domains.

[30] The crust-mantle boundary has been mapped in domain 1 only with PmP wide-angle reflection because MCS data are contaminated with multiple energies at Moho arrival time predicted by WAS modeling (blue line in Figures 4 and 6). In domains 2 and 4 both methods have detected the crust-mantle boundary and provide complementary information. The interpreted crust-mantle boundary appears in MCS image typically as a band of reflections that is ~0.2–0.5 s TWT thick, formed by individual events that are ~0.5–2 km long (Figure 5) and locally as subhorizontal reflections that may indicate a more abrupt boundary (e.g., CMPs 44,000–45,000). The band of reflections may be interpreted to represent a layered transition from crust to mantle rocks. In some areas the subhorizontal reflections form the base of a reflectivity package where gently dipping midcrustal reflections merge downdip (e.g., CMPs 47,000–42,000 and 17,000–14,000 in Figure 5).

[31] The crust along domains 2 and 4 displays a 7–9 km laterally rather constant thickness (Figure 3) that is displayed as a 2.5 to 2.9 s TWT thick crust in seismic images (Figure 5). Similar crustal structure and lower crustal reflectivity have been described in oceanic back-arc crust in the South Balearic basin [*Booth-Rea et al.*, 2007] and in—slightly thinner—oceanic crust formed at fast-spreading rates [*Ranero et al.*, 1997]. In these two settings the lower crustal structure has been interpreted as formed by either a lithological layering formed in a lower crustal magma chamber or a deformation fabric of such a lithological layering that has been transposed by ductile flow.

[32] The crust-mantle boundary location obtained by WAS modeling and converted to TWT systematically shows the Moho somewhat shallower than the base of the reflectivity band in MCS images (Figures 4–6). This observation has two potential explanations: (1) the package of reflections in
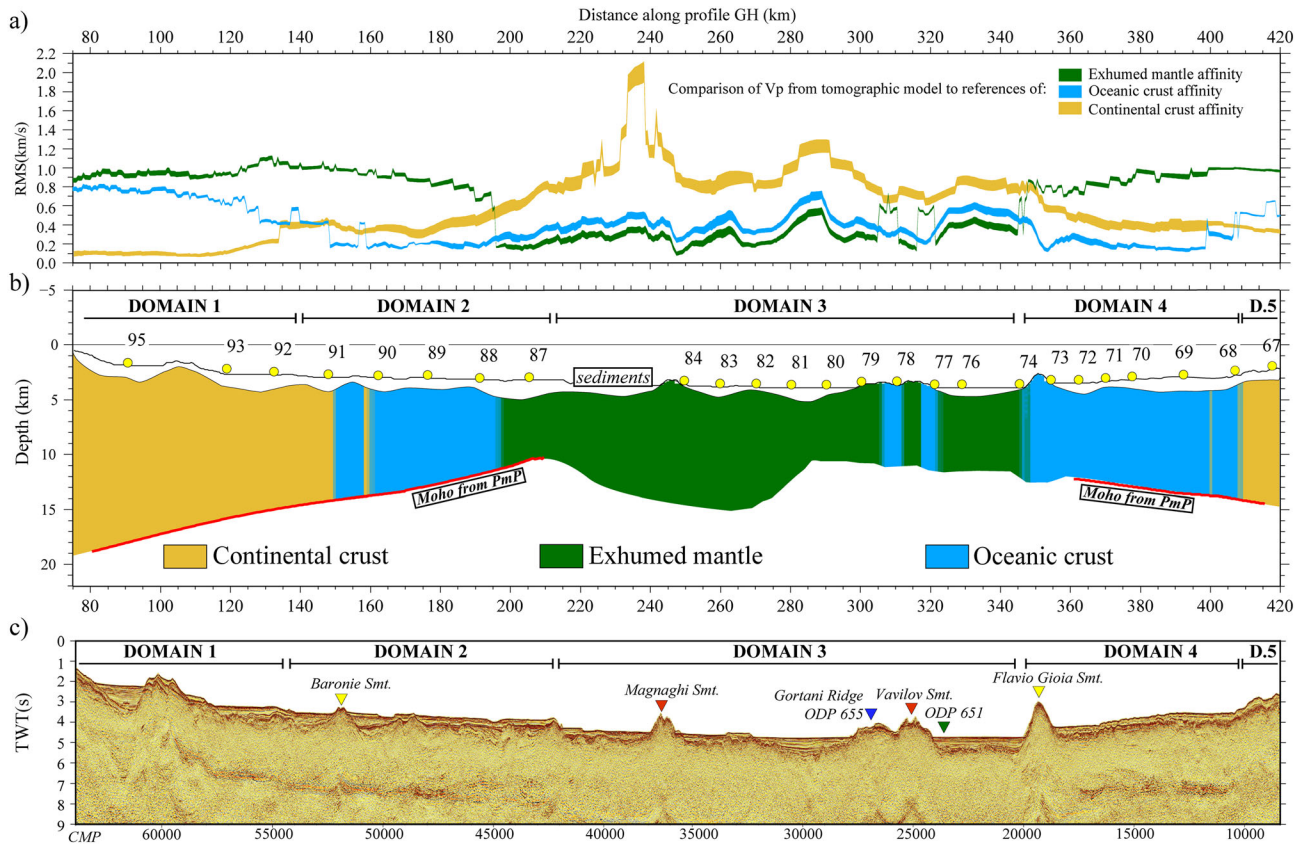
Figure 8. (a) Three velocity RMS values as a function of the distance along the tomographic model (Figure 3a) result from the automatic basement classification analysis (see section 4.3). The orange band represents the velocity RMS values result from the comparison of each 1-D velocity-depth profile of the tomographic model and the continental crust 1-D velocity-depth reference [*Christensen and Mooney*, 1995]. Similarly, the blue and green bands correspond to the RMSs values obtained from the comparison with a young (0–7 Ma) Atlantic oceanic crust [*White et al.*, 1992] and an exhumed mantle region [*Sallarès et al.*, 2013b], respectively. Details of the calculation are given in the text (see section 4.3). The thickness of each RMS line corresponds to the error bar obtained in the uncertainty analysis. Noteworthy is that the velocity values and gradients of oceanic (blue) and exhumed mantle (green) reference models are not distinguishable in the shallower 2 km, but clearly different at greater depths as it can be seen in Figure 7. This occurrence potentially causes the systematic similar trend between both RMS lines in the current automatic analysis. (b) Basement affinity model corresponding to the automatic basement classification explained in the text (see section 4.3) and shown in Figure 8a. The inverted Moho geometry (thick red line) and the location of the OBSs and OBHs (yellow circles) are also shown in the image. (c) MCS profile MEDOC 6 with the main morphological structures identified along the profile (e.g., Vavilov seamount), and the projections of ODP sites 655 and 651 [*Kastens and Mascle*, 1990]. The petrological nature of the basement is also represented by the same colored triangles as in Figure 1b (see legend in Figures 1b, 4, or 6) [*Dietrich et al.*, 1977; *Colantoni et al.*, 1981; *Kastens and Mascle*, 1990; *Sartori et al.*, 2004]. Vertical scale is exaggerated.

MCS images represents a layering with overall mantle velocities and the crust to mantle velocity transition is at its top, observed as the Moho location in the WAS; (2) alternatively, the TWT mismatch of Moho location in both data sets is due to seismic anisotropy [e.g., *Sallarès et al.*, 2013b]. This situation may arise when subhorizontal-propagating WAS waves travel faster than near-vertical MCS waves.

[33] Domain 3 shows neither wide-angle PmP reflections nor MCS images of the crust-mantle boundary, which strongly indicates that the increase from Vp < 8 km/s to Vp > 8 km/s is not an abrupt lithological boundary but a

gradual transition possibly over hundreds of meters that is expressed by the strong vertical velocity gradient (Figure 7).

[34] The tectonic structure of domain 1 is dominated by two large tilted fault-blocks (0–35 km) that bound a large half graben of the Sardinia basin (Figure 4). Tilting and top-basement geometry indicates that the structures formed by westward dipping faulting. The Sardinia basin contains a 0.5–0.7 s TWT package of strongly tilted strata, possibly deposited premain faulting that are themselves cut by minor faulting. The main half graben postfaulting infill is a sediment package ~1.3 s TWT thick at the depocenter. East of
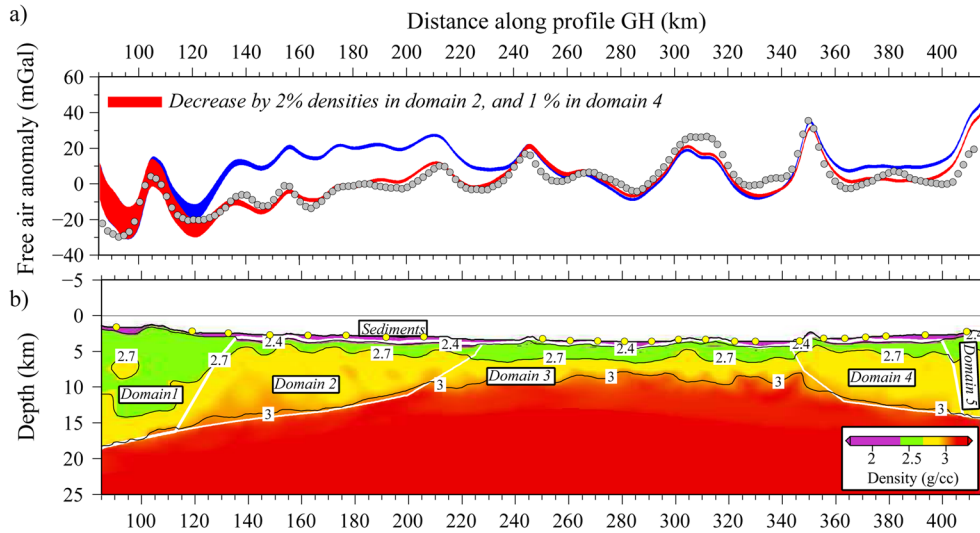
Figure 9. (a) Observed free-air gravity anomaly (grey circles) recorded during the MEDOC survey. Blue band corresponds to the gravity anomaly calculated from the velocity-derived density model obtained using *Hamilton*'s [1978] relationship for the sediment layer, *Christensen and Mooney*'s [1995] relationship for continental crust in domains 1 and 5, *Carlson and Herrick*'s [1990] relationship for oceanic crust in domains 2 and 4, and *Carlson and Miller*'s [2003] conversion law for partially serpentinized peridotites in domain 3. The RMS value for this case is 18 mGal. Red band corresponds to the gravity anomaly calculated from the density model obtained by using the same conversion laws as in the first case but decreasing by 2 and 1% densities in domains 2 and 4, respectively. The RMS value is 8 mGal. (b) Velocity-derived density model corresponding to the best fit (red band). Yellow circles show the location of the OBS and OBH.

Sardinia basin, the seismic image shows that the tectonic structure of domain 1 changes in fault polarity from west-dipping to east-dipping and remains constant across the Cornaglia Terrace in domain 2, with no abrupt structural changes (Figure 4).

[35] Domain 2 displays a tectonic structure fundamentally different compared to that of domain 1. The structure of domain 2 is characterized by comparatively wider spacing between fault blocks that in domain 1, indicating that faulting was less important during extension of domain 2. In domain 2 there are six main fault blocks with a maximum relief of a few hundreds of meters, bounded by eastward dipping normal faults (Figure 5). The largest and only fault block that crops out of the seafloor is the southernmost extension of the Baronie seamount (Figure 1b). The Baronie fault-block forms over 1 km of top-of-basement relief, and dredging indicates a continental origin [*Colantoni et al.*, 1981; *Sartori et al.*, 2004] so that is probably similar to blocks in domain 1. The rest of the fault blocks of domain 2 are considerably smaller in dimensions.

[36] Domain 3 across the Magnaghi and Vavilov basins is bounded on either end by two a set of major faults that dip with opposite directions on either side. However, the ~130 km wide domain 3 displays basically no evidence of high-angle normal faulting causing significant basement relief (Figures 4 and 6). The large relief in the map (Figure 1) corresponds to the 1–4 km tall basaltic Magnaghi and Vavilov seamounts (Figure 1b) and D'Ancona and Gortani Ridges. The deeper, smooth basement top of the Vavilov basin was drilled during ODP 651 near line MEDOC-6. Drilling recovered a few tens of meters of basalt overlying several tens of meters of mantle peridotite (Figure 1)

[*Kastens and Mascle*, 1990]. Domain 3 has neither Moho reflections in the MCS images nor PmP phases from Moho in the WAS records, which may indicate a different nature for the basement of this Domain (Figures 4 and 6).

[37] Domain 4 extends from ~275 to 330 km along the MCS profile, with a structure in the seismic image that resembles the structure of domain 2, but contains fewer, smaller-offset faults (Figures 4–6). The image shows a fairly smooth top of the basement, indicating minor tectonic extension during the creation of this region of the basin. The well-imaged lower crustal packages of reflections in the MCS data (Figure 5) and the spatially coincident PmP WAS reflections (Figure 6) clearly delineate the base of the crust as an abrupt seismic boundary for domain 4, which is in contrast to domain 3 but similarly to domain 2. The pattern of eastward dipping lower crustal reflections that merge with the base of the crust reflections in the MCS image is also similar to the structure of domain 2 (CMP 16,000 to 14,000 in Figure 5).

[38] The MCS image extends farther eastward that the WAS recordings and provides a wider coverage of domain 5 (Figure 3). The seismic image of domain 5 displays a progressive shoaling of the top of basement corresponding to a gradual landward thickening of the crust, as indicated by the WAS model (Figures 4 and 6). The crust is cut by numerous faults, including several large-offset normal faults that produce considerable top of basement relief. The tectonic structure of half and full grabens of few hundreds of meter to about 1 km deep indicates that extension by faulting was a comparatively important process during the opening of domain 5, similarly to domain 1 and in contrast to domains 2, 3, and 4.
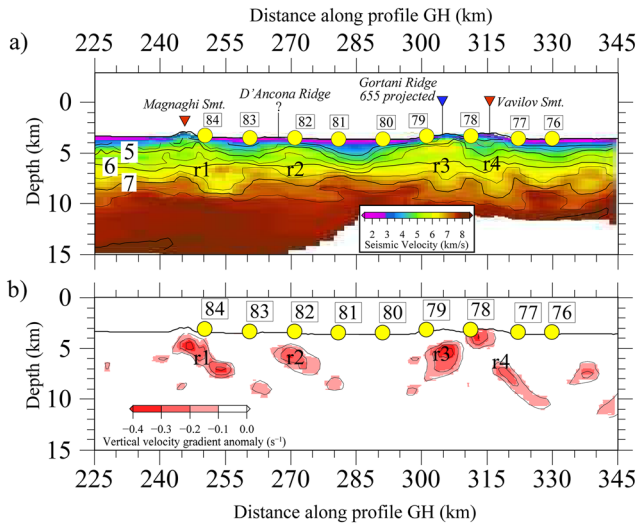
Figure 10. (a) Close-up of the tomographic model (Figure 3a) along the Magnaghi and Vavilov basins with the main morphological elements identified. The same colored triangles used in Figure 1b are also used in this image [*Dietrich et al.*, 1977; *Colantoni et al.*, 1981; *Kastens and Mascle*, 1990]. (b) Map of the vertical velocity gradient anomalies along the tomographic model, which has been obtained by comparing the vertical velocity gradient model, corresponding to the tomographic model (Figure 3a), with a laterally smoothed version of the same gradient model. The smoothing was done by applying a Gaussian filter with a horizontal correlation length of 15 km and a vertical one of 0.5 km. The goal of this method is to determine the dimensions of those velocity anomalies observed along the tomographic model (Figure 3a), which in this case might be representing the tomographic signature of the structure in depth of the Magnaghi seamount (r1), D'Ancona (r2) and Gortani (r3) ridges, and the Vavilov seamount (r4).

4.3. Automatized Interpretation of Basement Affinity Based on *P* Wave Depth-Velocity Profiles

[39] To reduce interpretation subjectivity, we have developed an independent method for the automatic classification of the petrological affinity of the structural domains based on velocity-depth relationships. The method consists of comparing 1-D velocity-depth profiles extracted from the 2-D tomographic model (Figure 3a) with compilations made for continental crust [*Christensen and Mooney*, 1995], oceanic crust [*White et al.*, 1992], and exhumed mantle [*Sallarès et al.*, 2013a] (Figure 8). We have calculated the RMS difference between 1-D velocity models along the 2-D profile (1-D profiles are calculated from 5 km wide averages of the 2-D velocity model) with the average of each of the three velocity-depth references [*White et al.*, 1992; *Christensen and Mooney*, 1995; *Sallarès et al.*, 2013a], assigning the affinity corresponding to that giving the smallest RMS. The results obtained from the comparison with continental crust, oceanic crust, and exhumed mantle are represented in Figure 8a.

[40] The smallest RMS at any point along the line automatically determines the basement affinity (Figure 8b). This method clearly separates basement type in the five

domains previously discussed in section 4.1. In domain 1, the reference model that best fits the velocity-depth profile is that of continental crust (Figures 8a and 8b). Domains 2 and 4, including the Cornaglia Terrace and the conjugate Campania Terrace, have velocities that fit better with the reference model of oceanic crust (Figure 8). However, in these two domains the lower crust has velocities that are systematically lower than typical, Atlantic-like, 0–7 Ma old oceanic crust (Figure 7) [*White et al.*, 1992]. The easternmost ~10 km of the profile matches better the continental crust reference, suggesting that the nature of domain 5 could be continental. This interpretation must be carefully taken since this region is poorly constrained by the WAS data. However *Biella et al.* [2007] shows that at about 90 km eastward OBH 66 the basement displays continental features. Interestingly, a narrow continental-affinity segment is discerned in domain 2, coinciding with the location of the Baronie seamount of known continental nature (Figure 8c) [*Sartori et al.*, 2004]. In domain 3 the velocity-depth profiles that match best clearly correspond to that of partially serpentinized peridotite (Figures 7 and 8b), with the exception of two narrow segments just below the Gortani Ridge and the Vavilov seamount, which are better explained by an oceanic crustal affinity (Figures 3a and 8b). These two seamounts have been previously described as basaltic edifices [*Robin et al.*, 1987; *Beccaluva et al.*, 1990; *Bertrand et al.*, 1990; *Savelli*, 2002], possibly intruding a basement made of serpentinized mantle rocks.

4.4. Density Structure

[41] In order to challenge the petrological interpretation described in the previous section (Figures 7 and 8), we have converted the velocities of the tomographic model (Figure 3a) into densities using the Vp-ρ relationships corresponding to the petrological affinities assigned by the automatized velocity analysis (Figure 8). Hence, the *Christensen and Mooney*'s [1995] Vp-ρ relationship for continental rocks was used in domains 1 and 5, *Carlson and Herrick*'s [1990] conversion law for oceanic crust in domains 2 and 4, and *Carlson and Miller* [2003] Vp-ρ relationship for partially serpentinized peridotites in domain 3. The gravity response of the resulting density model (Figure 9a) presents a slight mismatch of 18 mGal with the observed free-air gravity anomaly. A possible explanation for this mismatch is the anomalous lower crustal velocity in domains 2 and 4, which is systematically lower than a typical 0–7 Ma old oceanic crust [*White et al.*, 1992], possibly reflecting a different petrological composition. To correct this effect, we have decreased crustal densities by 1–2% in these two domains (Figure 9b). The obtained model fits remarkably well the observed gravity anomaly with an RMS of 8 mGal (Figure 9a).

5. Discussion

[42] In this section, we integrate the WAS model and MCS image, with the gravity modeling results to interpret the nature of the basement beneath the Sardinia margin (domain 1), Cornaglia Terrace (domain 2), Vavilov and Magnaghi basins (domain 3), Campania Terrace (domain 4), and the Campania margin (domain 5).
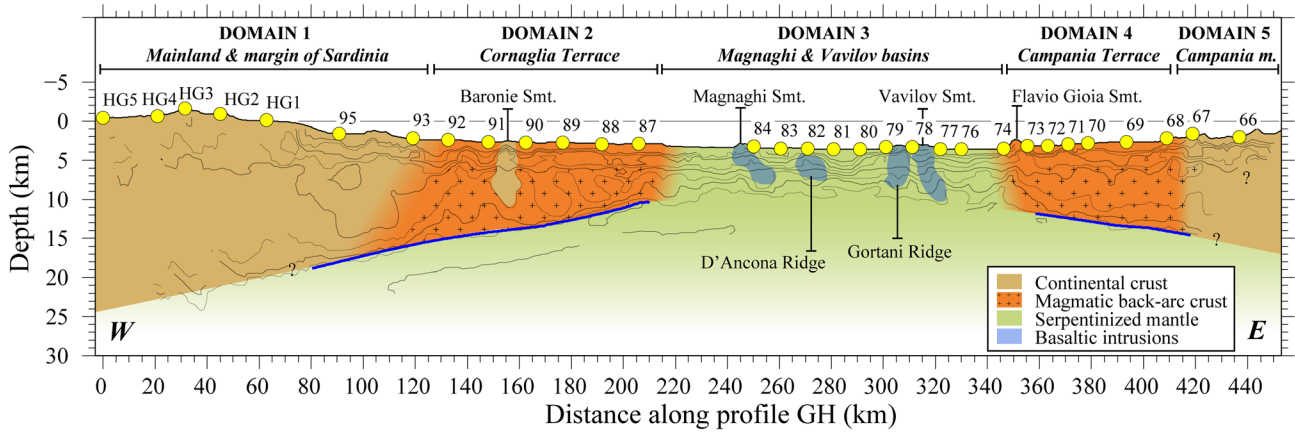
Figure 11. Interpretative cartoon of the main domains and the main magmatic and nonmagmatic bodies identified in this work along the WAS line GH, superimposed by the velocity contour lines of the tomographic model (Figure 3a). Blue line displays the location of the inverted Moho and yellow circles the location of the land stations and the OBS/H. Campania m.: Campania margin.

5.1. The Continental Margins of Sardinia (Domain 1) and Campania (Domain 5)

[43] The Sardinia Island and its margin (domain 1 in Figures 3a, 4, and 6) have a continental velocity and density structure (Figures 7 and 8). This interpretation is also consistent with regional geology. Field observations indicate that Sardinia basement is mainly formed by Paleozoic, locally Mesozoic and Eocene rocks from the European continental lithosphere, overlaid by—from bottom to top—continental-to-marine sediment sequence related to Oligocene-Miocene rifting [*Cherchi and Montadert*, 1982]. Similarly, dredged basement rocks of the Sardinia margin (Figures 1b, 4, and 5) include Late Paleozoic (~300 Ma) granitoids (e.g., Baronie seamount in Figures 3a and 5) of the Variscan orogeny [*Mascle and Rehault*, 1990; *Sartori et al.*, 2004], covered by Serravallian-early Tortonian to Pliocene-Pleistocene sediment [*Mascle and Rehault*, 1990; *Sartori*, 1990; *Sartori et al.*, 2004].

[44] The WAS data do not constrain well crustal thickness beneath the island, but complementary gravity modeling indicates a ≤24 km thickness, in agreement with previous seismic estimations [*Di Stefano et al.*, 2011]. Other WAS profiles acquired during the MEDOC-2010 experiment in the Northern Tyrrhenian basin, across Corsica and offshore to the east, suggests a similar thickness beneath the island [*Moeller et al.*, 2013]. The crystalline crust thins from ~15 km thick under the coastline (80 km, Figure 3a) to 9 km at domain 1 edge, implying a stretching factor (*ß*) of ~3 (125 km, Figure 3a). However, the transition between continental domains 1 and 2 along the transect is probably relatively abrupt as the automatic classification seems to indicate (Figure 8).

[45] Domain 5 (Campania margin) is less well characterized with WAS data because the line has mapped only the outer segment (Figure 3a) although it is also classified as continental (Figure 8). However, the MCS image extends further east and shows 60 km of a terrain characterized by significant extensional tectonics during formation. The structure of domain 5, with a rough, eastward shoaling relief, indicating a gradual eastward thickening of the crust (also mapped in the segment covered with the WAS line), is clearly differentiated from

domain 4. No basement samples from the margin have been reported in literature, and we interpret this segment as an extension of the continental crust of Italy mainland.

5.2. Magmatic Crust Under the Cornaglia Terrace (Domain 2) and Campania Terrace (Domain 4)

[46] In domains 2 and 4 there are two anomalously tall local highs, respectively, the Baronie and Flavio Gioia seamounts, where dredging recovered continental rocks (Figure 1b). These highs are narrow, and only Baronie shows well as continental in the automatized classification (Figure 8b). However, the rest of domains 2 and 4 do not appear as continental in the automatized classification. Under the Cornaglia Terrace (domain 2) and Campania Terrace (domain 4) (Figures 1b, 3a, and 4–6) the basement presents a two-layer seismic structure characterized by different vertical velocity gradients that resemble oceanic crust layer 2 and layer 3 typical structure but with somewhat slower velocity in the lower crust (Figure 7). Under the Cornaglia Terrace the velocity model shows east-dipping crustal-scale velocity anomalies perhaps linked to east-dipping crustal-scale faults observed in the upper crust in the MCS line (Figures 3a and 5). This might indicate that these faults may be reaching close to the crust-mantle boundary. In contrast, faulting in the Campania Terrace has smaller offset.

[47] The limited amount of extension by faulting in the Campania Terrace is accompanied by a velocity structure somewhat more homogeneous than in the Cornaglia Terrace (Figure 3a), although it displays similar velocity-depth profiles (Figure 7). Most lower crust velocity-depth profiles of both domains display velocities ranging between 6.5 and ~7.0 km/s, so they are between typical continental and oceanic (Figure 8a) [*Christensen and Mooney*, 1995; *White et al.*, 1992], with a few exceptions in domain 2 that may reach 7.1–7.2 km/s in the lowermost crust.

[48] Thus, in general the velocity-depth relationships in domains 2 and 4 agree better with that of oceanic crust (Figures 7 and 8). However, the crust in these two domains is slightly thicker than typical oceanic crust [*White et al.*, 1992], ranging between 7 and 9 km and locally reaching 12 km (Figure 3a). In addition, to obtain a good fit of the

gravity data in these two domains (Figure 9a) it is necessary to decrease the crustal densities obtained with the *Carlson and Herrick*'s [1990] Vp-ρ relationship for oceanic crust by 1–2% (Figure 9). This indicates a departure in mineral composition from typical mid-ocean ridge oceanic crust.

[49] A two-layer seismic structure with similarly slow lower crustal velocity and crustal thickness has been described in other back-arc extensional settings, such as Ligurian basin [*Gailler et al.*, 2009] and Lau basin [*Turner et al.*, 1999]. In Lau the seismic structure is attributed to volcanic intrusions into the lower crust during crustal extension [*Turner et al.*, 1999] and to oceanic crust in the Ligurian [*Gailler et al.*, 2009]. It has been suggested that the interaction between subduction-related hydrous flux melting and decompression melts under a back-arc spreading center system produce a rock composition more felsic than typical mid-ocean ridge basalts [*Dunn and Martinez*, 2011].

[50] We, therefore, propose that the two-layer seismic structure under the Cornaglia Terrace and Campania Terrace (Figures 3a and 7) probably formed during the first phases of back-arc spreading at a distance of the volcanic arc close enough that there was an important contribution of subduction-related magmatism during crustal accretion [*Martinez et al.*, 2007].

5.3. Mantle-Rock Basement at Magnaghi and Vavilov Basins (Domain 3)

[51] Magnaghi and Vavilov basins (domain 3) are the segment that do not display Moho reflections in either MCS (Figures 4 and 6) or WAS data (Figures 2d, 2e, and 3a) and show the strongest vertical velocity gradients (Figure 7). The basement classification based on velocity-depth profiles indicates that the seismic structure is analogous to the continental-ocean transition of the West Iberia margin where the basement is made of mantle with no overlay of crustal-type rocks [*Dean et al.*, 2000; *Sallarès et al.*, 2013a]. The velocity uncertainty is small enough to discard that it might correspond to 0–7 Ma old oceanic crust (Figure 7) [*White et al.*, 1992]. These results, together with the good fit of the gravity data using *Carlson and Miller*'s [2003] conversion law for partially serpentinized peridotites (Figure 9), strongly indicate that the basement is made of mantle rocks with no detectable igneous crust carapace.

[52] In contrast with this interpretation, 1-D *P* wave velocity models obtained by forward modeling from WAS data recorded by deep-ocean geophones and seismographs between the 60's and the 80's (Figure 1a) [*Fahlquist and Hersey*, 1969; *Nicolich*, 1981; *Recq et al.*, 1984; *Duschenes et al.*, 1986] were interpreted as indicating that the Magnaghi and Vavilov basins are floored by oceanic crust. Nonetheless, the spatial density of deep-ocean receivers in these studies was much lower (approximately five receivers per 100 km of profile) than in the MEDOC experiment (Figures 1b and 3a), and shot-spacing was 10 times larger than in the MEDOC WAS lines [*Duschenes et al.*, 1986], so that the resolution and velocity control in our models is far better as demonstrated by the uncertainty analysis.

[53] Additionally, there is some evidence of igneous rocks in the basin that include the E-MOR basalts drilled on top of the Gortani Ridge (ODP site 655) and at the basement of the Vavilov basin (ODP site 651) (Figures 1b, 4, and 6) [*Beccaluva et al.*, 1990; *Bertrand et al.*, 1990; *Savelli*,

2002]. The Gortani Ridge is intersected by the tomographic model (between OBH79 and 80 in Figures 1b and 3a) and consequently imaged in depth (at ~300 km in Figure 3a). The velocity model shows that its crustal structure is anomalous and local (Figure 10), and it is not representative of the nature of the whole domain. The interpretation on its nature and origin is discussed in the next section.

[54] Concerning the oceanic-like nature of rocks of the Vavilov basin, E-MOR basalts drilled in this region are underlain by serpentinized peridotites, being this the lithological composition of the last unit in the borehole (ODP site 651 in Figures 1b, 4, and 6) [*Bonatti et al.*, 1990; *Kastens and Mascle*, 1990]. Other magmatic intrusions are present along this domain (i.e., Magnaghi and Vavilov seamounts.) (Figures 3a and 10); however, based on their affinity (alkaline) and age (3–0.1 Ma), we may conclude that they are not representative of oceanic accretion related to the opening of the Magnaghi and the Vavilov basins [*Robin et al.*, 1987; *Savelli*, 2002], but they likely represent later episodes of magmatic activity that intruded the original basement made of mantle rocks.

[55] On the basis of these observations, we interpret that the basement beneath domain 3 is mainly constituted by serpentinized peridotites locally intruded and overlaid by ocean-like basalts (i.e., E-MOR basalts). The strong vertical velocity gradient in the uppermost 3–4 km of the basement ($> 1\,s^{-1}$), the smoother velocity gradient just beneath, the velocities lower than those characteristic of unaltered mantle (< 8.2 km/s), and the absence of the Moho (Figures 3a and 6) are common features that have also been observed off Western Iberia [*Pinheiro et al.*, 1992; *Chian et al.*, 1999; *Dean et al.*, 2000; *Sallarès et al.*, 2013a]. In that region, the strong velocity gradient of the uppermost 3–4 km of the basement is attributed to an abrupt decrease in degree of serpentinization with depth (e.g., from >80% of serpentinization to 30–20% in less than 2 km), whereas the underlying smoother velocity gradient would correspond to a weakly serpentinized mantle [*Sallarès et al.*, 2013b].

5.4. Volcanic Intrusions in Mantle-Rock Basement

[56] Throughout domain 3, and coinciding with the location of the magmatic edifices of the Magnaghi and Vavilov seamounts, the D'Ancona Ridge and the southernmost part of the Gortani Ridge, the tomographic model displays several vertically elongated velocity anomalies characterized by a gentler vertical velocity gradient as compared with the rest of this domain (e.g., at ~300 km in Figures 10a and 11). In order to improve the definition of these velocity anomalies, we have compared the vertical velocity gradient model obtained from the tomographic model (Figure 3a) with a laterally smoothed version of the same vertical velocity gradient model, excluding the sedimentary layer. As a result, we obtained anomalies where the vertical gradient is smoother than the background gradient. As can be seen in Figure 10b, these anomalies concentrate under the volcanic centers (r1, r2, r3, and r4 in Figure 10b).

[57] We interpret the subvertical anomaly r1 (Figure 10b), one of the strongest anomalies in the tomographic model ($<-0.3\,s^{-1}$), as the root of the magmatic body corresponding to the Magnaghi seamount, which has been sampled and dated at 3.0–2.7 Ma [*Savelli*, 2002].

[58] Anomaly r2 (Figure 10b) occurs under the intersection of the D'Ancona Ridge with the WAS line (Figures 1b and 10). This ridge, which has not been sampled, has been generally interpreted as a faulted continental block, although a possible magmatic origin has also been suggested [*Marani and Gamberi*, 2004; *Sartori et al.*, 2004]. On the basis of its location and given that the velocity gradient below it is rather high in comparison to that of a continental block (e.g., Baronie seamount at 150 km of profile in Figure 3a), we suggest that it might also correspond to a basaltic intrusion into the mantle basement forming the root of a volcanic edifice.

[59] We interpret anomaly r3 (Figure 10b) as the root of the Gortani Ridge. This ridge is composed by E-MOR basalts (ODP site 655) dated at 4.3 Ma [*Beccaluva et al.*, 1990; *Bertrand et al.*, 1990; *Savelli*, 2002], being the oldest magmatic body imaged in the central basin but younger than the opening of the Vavilov basin where it intrudes.

[60] Anomaly r4 (Figure 10b) is located below the northernmost intersection of Vavilov seamount, likely representing a related intrusion. Similarly to Magnaghi seamount, Vavilov seamount is related to intraplate magmatism created at 2.6–0.1 Ma after the end of extension in the central basin [*Robin et al.*, 1987; *Savelli*, 2002].

5.5. Implications of the New Geological Domains Defined in the Central Tyrrhenian Sea

[61] The interpretation of the velocity, density, and tectonic structure obtained with the MEDOC experiment WAS, gravity, and MCS data has led to a radically new definition of geological domains in the Central Tyrrhenian basin (Figure 11).

[62] Previous interpretations of Cornaglia and the new-defined Campania Terraces assumed a basement formed by stretched continental crust (Figure 1b) [e.g., *Duschenes et al.*, 1986; *Sartori et al.*, 2004]. However, the two-layer velocity structure in those two regions fits better with that of oceanic crust. The depth-velocity distribution indicates that the lower crust velocity is slightly slower than typical oceanic layer 3. We interpret that the oceanic-type crust structure formed in a back-arc spreading setting influenced by flux melting related with the dehydration of the subducted Ionian slab, similar to what has been described in other back-arc basins in the Pacific (Figure 8, 9, and 11) [*Martinez et al.*, 2007; *Dunn and Martinez*, 2011].

[63] Previous interpretations of the Magnaghi and the Vavilov basins assumed that they were floored by oceanic crust [*Kastens and Mascle*, 1990; *Sartori et al.*, 2004; *Cella et al.*, 2008] and that the serpentinized peridoties cored in ODP 651 (Figure 1b) might correspond to an isolated continental block that contain a sliver of Tethyan ophiolite [*Kastens and Mascle*, 1990]. As a result most maps from the region typically display ocean crust in these basins. In contrast, we suggest that the basement of Magnaghi and Vavilov basins is fundamentally composed by mantle peridotites serpentinized to 5–6 km depth under the sediment cover. These altered mantle rocks are locally intersected by magmatic intrusions of basaltic affinity that form the root of volcanic constructions of Magnaghi and Vavilov seamounts and D'Ancona and Gortani Ridges (Figure 10).

[64] Results obtained along this transect of the MEDOC experiment show that the Sardinia and Campania conjugate margins are formed by extended continental crust of overall crustal and tectonic asymmetric structures. The joint analysis of velocities and densities with observations of the tectonic structure show how both continental margins rather abruptly transition to what has been interpreted as oceanic back-arc crust in the Cornaglia and Campania Terraces. Finally, in contrast to what has been previously proposed, the back-arc oceanic crust under both terraces give up in the center of the basin to exhumed mantle rocks of the Magnaghi and Vavilov basins.

[65] The structure defined with our data set indicates a spatial distribution of rock types that implies a temporal basin evolution from an extending continental crust to back-arc oceanic crust formation and to mantle exhumation. This spatial distribution of crust types and the inferred temporal evolution are in stark contrast to current models of lithospheric extension and rifting in systems where mantle unroofing is interpreted to have occurred (e.g., North Atlantic rifted margins, *Ranero and Pérez-Gussinyé*, 2010). Commonly accepted models studying the continent to ocean transition (involving mantle unroofing) typically postulate a continuum from continental crust extension, mantle exhumation, and eventual oceanic crust formation by gradual instauration of a decompression melt system [e.g., *Pérez-Gussinyé et al.*, 2006]. However, we speculate that currently accepted models of lithospheric extension and formation of a spreading center are based on too limited data sets with modern, high-quality seismic observations. Our results indicate that further geophysical experiments sampling different rifting systems with closely spaced OBSs and coincident MCS data are needed to understand the possible spectrum of crustal structures and the corresponding rifting processes.

6. Conclusions

[66] The results obtained with WAS and gravity modeling, together with the observations made from the MCS profile reveal three geological affinities of the basement from Sardinia to the Campania margin (Figure 11).

[67] Continental crust is observed in domains 1 and 5 (Figure 11). Domain 1 is formed by continental crust of Sardinia and Sardinia margin, which is characterized by landward and seaward normal faults and crustal thinning from ~22 km to ~13 km. The conjugate margin of Campania (domain 5) might represent the westernmost part of the Italian continental crust.

[68] The igneous crust is represented by the Cornaglia Terrace (domain 2) and the Campania Terrace (domain 4) (Figures 3a and 11). The transition between continental and magmatic crust is only observed by a marked, abrupt increase of velocities (> 7 km/s) in the lower crust (at 125 km in Figure 3a). Large-scale normal faulting has affected Cornaglia Terrace (Figure 5), whereas in the Campania Terrace, normal faulting is minor (Figures 3a, 4, and 5). The crustal structure in both regions is represented by velocities slightly lower than those found in a 0–7 Ma old-oceanic crust [*White et al.*, 1992] that we interpret as indicative of back-arc spreading close to the active volcanic arc.

[69] Domain 3 is interpreted as formed by exhumed mantle rocks. The main characteristics are the lack of Moho reflections in both WAS and MCS data and by a vertical velocity structure similar to other regions where basement is made of serpentinized mantle [*Dean et al.*, 2000; *Sallarès et al.*, 2013b]. Along this domain the tomographic model displays

vertically elongated velocity anomalies interpreted as basaltic bodies that intrude the mantle and are the root of the Magnaghi and Vavilov seamounts and Gortani and D'Ancona Ridges.

[70] In summary, according to our models, rifting in the Central Tyrrhenian basin would have started with continental crust extension, continued with back-arc spreading leading to generation of igneous back-arc crust, followed by nearby mantle exhumation intruded by later magmatic episodes. Our detailed analysis provides a new configuration of the type of basement that with further results of the MEDOC project [e.g., *Moeller et al.*, 2013] will allow to define a genetic model of this region. The interpretation of these results differ from current conceptual models of the formation of rifting systems involving mantle exhumation and indicate that the response of the continental lithosphere to extension processes may be more complex than previously assumed.

References

Barberi, F., H. Bizouard, G. Capaldi, G. Ferrara, R. Gasparini, R. Innocenti, J. L. Joron, B. Lambret, M. Treuil, and C. Allegre (1978), Age and nature of basalts from the Tyrrhenian Abyssal Plain, in *Init. Repts. of the DSDP*, vol. 42(Pt. 1) edited by K. Hsu et al., pp. 509–514, U.S. Govt. Printing Office, Washington, D.C.

Bartole, R. (1995), The Norht Tyrrhenian-Northern Apennines post-collisional system: Constraints for a geodynamic model, *Terra Nova*, 7, 7–30.

Beccaluva, L., et al. (1990), Geochemistry and mineralogy of volcanic rocks from the ODP sites 650, 651, 655 and 654 in the Tyrrhenian Sea, in *Proceedings of the Ocean Drilling Program. Scientific Results*, vol. 107, edited by K. A. Kastens et al., pp. 49–74, U.S. Gov. Print. Off., Washington, D. C.

Bertrand, H., P. Boivin, and C. Robin (1990), Petrology and geochemistry of basalts from the Vavilov basin (Tyrrhenian Sea), Ocean Drilling Program Leg 107, Holes 651A and 655, in *Proceedings of the Ocean Drilling Program. Scientific Results*, vol. 107, edited by K. A. Kastens et al., pp. 75–92, U.S. Gov. Print. Off., Washington, D. C.

Biella, G., R. de Franco, E. Marsella, and G. Caielli (2007), Deep structures in Southern Italy. Evidences from the Gargano-Pantelleria seismic refraction experiment (1971), *Boll. Soc. Geol. It. (It.J.Geo.sci.)*, 7, 163–175.

Bonatti, E., M. Seyler, J. Channell, J. Girardeau, and G. Mascle (1990), Peridotites drilled from the Tyrrhenian Sea, ODP Leg 107, in *Proceedings of the Ocean Drilling Program Scientific Results*, vol. 107, edited by K. A. Kastens et al., pp. 37–48, U.S. Gov. Print. Off., Washington, D. C.

Booth-Rea, G., C. R. Ranero, J. M. Martínez-Martínez, and I. Grevemeyer (2007), Crustal types and Tertiary tectonic evolution of the Alborán Sea, western Mediterranean, *Geochem. Geophys. Geosyst.*, 8, Q10005, doi:10.1029/2007GC001639.

Carlson, R. L., and C. N. Herrick (1990), Densities and porosities in the oceanic crust and their variations with depth and age, *J. Geophys. Res.*, 95(B6), 9153–9170.

Carlson, R. L., and D. J. Miller (2003), Mantle wedge water contents estimated from seismic velocities in partially serpentinized peridotites, *Geophys. Res. Lett.*, 30(5), 1250, doi:10.1029/2002GL016600.

Cella, F., M. Fedi, G. Florio, V. Paoletti, and A. Rapolla (2008), A review of the gravity and magnetic studies in the Tyrrhenian basin and its volcanic districts, *Ann. Geophys.*, 51(1), doi:10.4401/ag-3035

Cherchi, A., and L. Montadert (1982), Oligo-Miocene rift of Sardinia and the early history of the western Mediterranean basin, *Nature*, 298, 736–739.

Chian, D., K. E. Louden, T. A. Minshull, and R. B. Whitmarsh (1999), Deep structure of the ocean-continent transition in the southern Iberia Abyssal Plain from seismic refraction profiles: Ocean Drilling Program (Legs 149 and 173) transect, *J. Geophys. Res.*, 104(B4), 7443–7462.

Christensen, N., and W. Mooney (1995), Seismic velocity structure and composition of the continental crust: A global view, *J. Geophys. Res.*, 100(B7), 9761–9788, doi:10.1029/95JB00259.

Colantoni P., A. Fabbri, P. Gallignani, R. Sartori, and J. P. Rehault (1981), Carta Litologica e Stratigrafica dei Mari Italiani, scala 1/1.500.000, Litografia Artistica Cartografica, Firenze, Italy.

Contrucci, I., A. Nercessian, N. Béthoux, A. Mauffret, and G. Pascal (2001), A Ligurian (Western Mediterranean Sea) geophysical transect revisted, *Geophys. J. Int.*, 146, 74–97.

Contrucci, I., A. Mauffret, C. Brunet, A. Nercessian, N. Béthoux, and J. Ferrandini (2005), Deep structure of the North Tyrrhenian Sea from multi-channel seismic profiles and on land wide angle reflection/refraction seismic recording (LISA cruise): Geodynamical implications, *Tectonophysics*, 406(3–4), 141–163, doi:10.1016/j.tecto.2005.05.015.

Dean, S. M., T. A. Minshull, R. B. Whitmarsh, and K. E. Louden (2000), Deep structure of the ocean-continent transition in the southern Iberia abyssal plain from seismic refraction profiles: The IAM-9 transect at 40° 20′N, *J. Geophys. Res.*, 105(B3), 5859–5885.

Dewey, J. F., M. L. Helman, E. Turco, D. H. W. Hutton, and S. D. Knott (1989), Kinematics of the western Mediterranean, in *Alpine Tectonics*, vol. 45, edited by P. Cowardm, D. Dietrich, and G. Park, pp. 265–283, Geological Society Special Publication, London.

Di Stefano, R., I. Bianchi, M. G. Ciaccio, G. Carrara, and E. Kissling (2011), Three-dimensional Moho topography in Italy: New constraints from receiver functions and controlled source seismology, *Geochem. Geophys. Geosyst.*, 12, Q09006, doi:10.1029/2011GC003649.

Dietrich, V., R. Emmermann, J. Keller, and H. Puchelt (1977), Tholeitic basalts from the Tyrrhenian sea floor, *Earth Planet Sci. Lett.*, 36, 285–296.

Dunn, R. A., and F. Martinez (2011), Contrasting crustal production and rapid mantle transitions beneath back-arc ridges, *Nature*, 469, 198–202, doi:10.1038/nature09690.

Duschenes, J., M. C. Sinha, and K. E. Louden (1986), A seismic refraction experiment in the Tyrrhenian Sea, *Geophys. J. R. Astron. Soc.*, 85, 139–160.

Faccena, C., T. W. Becker, F. P. Lucente, L. Jolivet, and F. Rossetti (2001), History of subduction and back-arc extension in the Central Mediterranean, *Geophys. J. Int.*, 145, 809–820.

Fahlquist, D. A., and J. B. Hersey (1969), Seismic refraction measurements in the Western Mediterranean Sea, *Bull. Insr. Oceanogr. Monaco*, 67, l–52.

Finetti, I. R., M. Boccaletti, M. Bonini, A. Del Ben, R. Geletti, M. Pipan, and F. Sani (2001), Crustal section based on CROP seismic data across the North Tyrrhenian-Northern Apennines-Adriatic Sea, *Tectonophysics*, 343, 135–163.

Gailler, A., F. Klingelhoefer, J.-L. Olivet, and D. Aslanian (2009), Crustal structure of a young margin pair: New results across the Liguro-Provençcal Basin from wide-angle seismic tomography, *Earth Planet Sci. Lett.*, 289, 333–345, doi:10.1016/j.epsl.2009.07.001.

Gallart, J., N. Vidal, A. Estévez, J. Pous, F. Sàbat, C. Santisteban, E. Suriñach, and the ESCI-València Trough Group (1995), The ESCI-Vlència Trough vertical reflection experiment: A seismic image of the crust from the NE Iberian Peninsula to the Western Mediterranean, *Rev. Soc. Geol. España*, 8(4), 401–415.

Gattacceca, J., A. Deino, R. Rizzo, D. S. Jones, B. Henry, B. Beaudoin, and F. Vadeboin (2007), Miocene rotation of Sardinia: New paleomagnetic and geochronological constraints and geodynamic implications, *Earth Planet Sci. Lett.*, 258, 359–377, doi:10.1016/j.epsl.2007.02.003.

Gvirtzman, Z., and A. Nur (2001), Residual topography, lithospheric structure and sunken slabs in the central Mediterranean, *Earth Planet. Sci. Lett.*, 187, pp. 117–130.

Hamilton, E. L. (1978), Sound velocity-density relations in sea-floor sediments and rocks, *J. Acoust. Soc. Am.*, 63, 366–377.

Kastens, K., and J. Mascle (1990), The geological evolution of the Tyrrhenian Sea: An introduction to the scientific results of ODP LEG 107, in *Proceedings of the Ocean Drilling Program. Scientific Results*, vol. 107, edited by K. A. Kastens et al., pp. 3–26, Ocean Drilling Program, College Station, Texas, U.S.A.

Kern, H., and J. M. Tubia (1993), Pressure and temperature dependence of P- and S-wave velocities, seismic anisotropy and density of sheared rocks from the Sierra Alpujata massif (Ronda peridotites, Southern Spain), *Earth Planet Sci. Let.*, 119, 191–205.

Korenaga, J., W. S. Holbrook, G. M. Kent, P. B. Kelemen, R. S. Detrick, H.-C. Larsen, J. R. Hopper, and T. Dahl-Jensen (2000), Crustal structure of the southeast Greenland margin from joint refraction and reflection seismic tomography, *J. Geophys. Res.*, 105(B9), 21,591–21,614, doi:10.1029/2000JB900188.

Korenaga, J., W. S. Holbrook, R. S. Detrick, and P. B. Kelemen (2001), Gravity anomalies and crustal structure at the southeast Greenland margin, *J. Gophys. Res.*, 106(B5), 8853–8870.

Lustrino, M., S. Duggen, and C. L. Rosenberg (2011), The Central-Western Mediterranean: Anomalous igneous activity in an anomalous collisional tectonic setting, *Earth Sci. Rev.*, *104*, 1–40, doi:10.1016/j.earscirev.2010.08.002.

Malinverno, A., and W. B. F. Ryan (1986), Extension in the Tyrrhenian Sea and shortening in the Apennines as result of arc migration driven by sinking of the lithosphere, *Tectonics*, *5*(2), 227–245, doi:10.1029/TC005i002p00227.

Marani, M. P., and F. Gamberi (2004), Structural framework of the Tyrrhenian Sea unveiled by seafloor morphology, in *Memorie Descrittive Della Carta Geologica d'Itlaia, From Seafloor to Deep Mantle: Architecture of the Tyrrhenian Backarc Basin*, vol. LXIV, edited by P. Marani, F. Gamberi, and E. Bonatti, pp. 97–108, Servizio Geologico d'Italia.

Martinez, F., K. Okino, Y. Ohara, A.-L. Reysenbach, and S. K. Goffredi (2007), Back-arc basins, *Oceanography*, *20*(1), 116–127.

Mascle, J., and J.-P. Rehault (1990), A revised seismic stratigraphy of the Tyrrhenian Sea: Implications for the basin evolution, in *Proceedings of the Ocean Drilling Program. Scientific Results*, vol. 107, edited by K. A. Kastens et al., pp. 617–636, Ocean Drilling Program, College Station, TX.

Mauffret, A., and I. Contruccci (1999), Crustal structure of the North Tyrrhenian Sea: First results of the multichannel seismic LISA cruise, in *The Mediterranean Basins: Tertiary Extension Within the Alpine Orogen*, vol. 156, edited by B. Durand et al., pp. 169–193, Geological Society London, Special Publications, London.

Moeller, S., I. Grevemeyer, C. R. Ranero, C. Berndt, D. Klaeschen, V. Sallarès, N. Zitellini, and R. de Franco (2013), Rifted structure in the northern Tyrrhenian Sea Basin: Results from a combined wide-angle and multichannel seismic study, *Geochem. Geophys. Geosyst.*, doi:10.1002/ggge.20180.

Moser, T. J. (1991), Shortest path calculation of seismic rays, *Geophysics*, *56*, 59–67.

Moser, T. J., G. Nolet, and R. Snieder (1992), Ray bending revisited, *Bull. Seismol. Soc. Am.*, *82*, 259–288.

Nicolich, R. (1981), Il profilo Latina-Pescara e le registrazione mediante OBS nel mar Tirreno, in *1 ° Convegno del Gruppo Nazionale Geofisica Terra Solida*, vol. 2, pp. 621–637, CNR, Rome.

Nur, A., J. Dvorkin, G. Mavko, and Z. Ben-Avraham (1993), Speculations on the origins and fate of backarc basins, *Ann. Geofis.*, *36*, 155–163.

Parker, R. L. (1972), The rapid calculation of potential anomalies, *Geophys. J. R. Astron. Soc.*, *31*, 447–455.

Pascal, G., M. Torné, P. Buhl, A. B. Watts, and A. Mauffret (1992), Crustal and velocity structure of the Valencia trough (western Mediterranean), Part II. Detailed interpretation of five Expanded Spread Profiles, *Tectonophysics*, *203*, 21–35.

Pérez-Gussinyé, M., J. P. Morgan, T. J. Reston, and C. R. Ranero (2006), The rift to drift transition at non-volcanic margins: Insights from numerical modeling, *Earth Planet. Sci. Lett.*, *244*, 458–473, doi:10.1016/j.epsl.2006.01.059.

Pinheiro, L. M., R. B. Whitmarsh, and P. R. Miles (1992), The ocean-continent boundary off the western continental margin of Iberia-II. Crustal structure in the Tagus Abyssal Plain, *Geophys. J. Int.*, *109*, 106–124.

Ranero, C. R., and M. Perez-Gussinye (2010), Sequential faulting explains the asymmetry and extension discrepancy of conjugate margins, *Nature*, 294–299, doi:10.1038/nature09520.

Ranero, C. R., T. J. Reston, I. Belykh, and H. Gnibidenko (1997), Reflective oceanic crust formed at a fast-spreading center in the Pacific, *Geology*, *25*, 499–502.

Recq, M., J. P. Rehault, L. Steinmetz, and A. Fabbri (1984), Amincissement de la croute et accretion au centre du basin Tyrrhénien d'après la sismique refraction, *Mar. Geol.*, *85*, 411–428.

Robin, C., P. Colantoni, M. Gennesseaux, and J. P. Rehault (1987), Vavilov seamount: A mildly alkaline Quaternary volcano in the Tyrrhenian basin, *Mar. Geol.*, *78*, 125–136.

Rollet, N., J. Déverchère, M.-O. Beslier, P. Guennoc, J.-P. Rehault, M. Sosson, and C. Truffert (2002), Back-arc extension, tectonic inheritance, and volcanism in the Ligurian Sea, Western Mediterranean, *Tectonics*, *21*(3), 1015 doi:10.1029/2001TC900027.

Royden, L. H. (1993), The tectonic expression slab pull at continental convergent boundaries, *Tectonics*, *12*(2), 303–325.

Sallarès, V., and C. R. Ranero (2005), Structure and tectonics of the erosional convergent margin off Antofagasta, north Chile (23_300S), *J. Geophys. Res.*, *110*, B06101, doi:10.1029/2004JB003418.

Sallarès, V., J. J. Danobeitia, and E. R. Flueh (2000), Seismic tomography with local earthquakes in Costa Rica, *Tectonophysics*, *329*(1), 61–78, doi:10.1016/S0040-1951(00)00188-8.

Sallarès, V., A. Gailler, M.-A. Gutscher, D. Graindorge, R. Bartolomé, E. Gràcia, J. Díaz, J. J. Dañobeitia, and N. Zitellini (2011), Seismic evidence for the presence of Jurassic oceanic crust in the central Gulf of Cadiz (SW Iberian margin), *Earth Planet. Sci. Lett.*, doi:10.1016/j.epsl.2011.09.003.

Sallarès, V., S. Martinez-Loriente, M. Prada, E. Gràcia, C. R. Ranero, M.-A. Gutscher, R. Bartolomé, A. Gailler, J. J. Dañobeitia, and N. Zitellini (2013a), Seismic evidence of exhumed mantle rock basement at the Gorringe Bank and the adjacent Horseshoe and Tagus abyssal plains (SW Iberia), *Earth Planet Sci. Let.*, *365*, 120–131, doi:10.1016/j.epsl.2013.01.021.

Sallarès, V., A. Meléndez, M. Prada, C. R. Ranero, K. McIntosh, and I. Grevemeyer (2013b), Overriding plate of the Nicaragua convergent margin: Relationship to the seismogenic zone of the 1992 tsunami earthquake, *Geochem. Geophys. Geosyst.*, *14*, 3436–3461, doi:10.1002/ggge.20214.

Sartori, R. (1990), The main results of ODP Leg 107 in the frame of Neogene to Recent geology of perityrrhenian areas, in *Proceedings of the Ocean Drilling Program. Scientific Results*, vol. 107, edited by K. A. Kastens et al., pp. 715–730, Geological Society, London, Special Publications, London.

Sartori, R. (2003), The Tyrrhenian back-arc basin and subduction of the Ionian lithosphere, *Episodes*, *26*(3), 217–221.

Sartori, R., C. Carrara, L. Torelli, and N. Zitellini (2001), Neogene evolution of the southwestern Tyrrhenian Sea (Sardinia Basin and western Bathyal Plain), *Mar. Geol.*, *175*, 47–66.

Sartori, R., L. Torelli, N. Zitellini, G. Carrara, M. Matteo, and P. Mussoni (2004), Crustal features along a W–E Tyrrhenian transect from Sardinia to Campania margins (Central Mediterranean), *Tectonophysics*, *383*(3–4), 171–192, doi:10.1016/j.tecto.2004.02.008.

Savelli, C. (1988), Late Oligocene to Recent episodes of magmatism in and around the Tyrrhenian sea: Implications for the processes of opening in a young inter-arc basin of intra-orogenic (Mediterranean) type, *Tectonophysics*, *146*, 163–181.

Savelli, C. (2002), Time-space distribution of magmatic activity in the western Mediterranean and peripheral orogens during the past 30 Ma (a stimulus to geodynamic considerations), *J. Geodyn.*, *34*, 99–126.

Schettino, A., and E. Turco (2011), Tectonic history of the western Tethys since the Late Triassic, *Geol. Soc. Am. Bull.*, *123*(1/2), 89–105, doi:10.1130/B30064.1.

Steinmetz, L., F. Ferrucci, A. Hirn, C. Morelli, and R. Nicolich (1983), A 550 km long Moho traverse in the Tyrrhenian Sea from O.B.S. Recorded Pn waves, *Geophys. Res. Lett.*, *10*(6), 428–431.

Tarantola, A. (1987), *Inverse Problem Theory: Methods for Data Fitting and Model Parameter Estimation*, pp. 613, Elsevier Science, New York.

Toomey, D. R., and G. R. Foulger (1989), Tomographic inversion of local earthquake data from Hengill-Grensdalur central volcano complex, Iceland, *J. Geophys. Res.*, *94*, 17,497–17,510.

Trincardi, F., and N. Zitellini (1987), The rifting of the Tyrrhenian Basin, *Geo Mar. Lett.*, *7*, 1–6, doi:10.1007/BF02310459.

Turner, I. M., C. Peirce, and M. C. Sinha (1999), Seismic imaging of the axial region of the Valu Fa Ridge, Lau Basin—The accretionary processes of an intermediate back-arc spreading ridge, *Geophys. J. Int.*, *138*, 495–519.

Vignaroli, G., C. Faccena, F. Rossetti, and L. Jolivet (2009), Insights from the Apennines metamorphic complexes and their bearing on the kinematics evolution of the orogen, in *Collision and Collapse at the Africa-Arabia-Eurasia Subduction Zone*, vol. 311, edited by D. J. J. Van Hinsbergen, M. A. Edwards, and R. Govers, pp. 235–256, The Geological Society, London, Special Publications, London.

White, R. S., D. McKenzie, and R. K. O'Nions (1992), Oceanic crustal thickness from seismic measurements and rare earth element inversions, *J. Geophys. Res.*, *97*(B13), 19,683–19,715.

Zitellini, N., F. Trincardi, M. Marani, and A. Fabbri (1986), Neogene tectonics of the northern Tyrrhenian Sea, *Giorn. Geol*, *48*(1), 2.